

1 **Multi-ancestry proteome-phenome-wide Mendelian randomization offers a comprehensive**
2 **protein-disease atlas and potential therapeutic targets**
3

4 Chen-Yang Su¹⁻³, Adriaan van der Graaf⁴, Wenmin Zhang⁵, Dong-Keun Jang⁶, Susannah
5 Selber-Hnatiw^{1,2,7}, Ta-Yu Yang⁸, Guillaume Butler-Laporte^{3,9}, Kevin Y. H. Liang^{3,9}, Yiheng
6 Chen^{9,10}, Fumihiko Matsuda⁸, Maria C. Costanzo⁶, J. Brent Richards^{3,7,9-12}, Noel P. Burt⁶,
7 Jason Flannick^{6,13}, Sirui Zhou^{1-3,7}, Vincent Mooser^{1,2,7}, Tianyuan Lu^{14-17*}, Satoshi Yoshiji^{1-3,6,7,9*}
8

9 ¹Canada Excellence Research Chair in Genomic Medicine, McGill University, Montréal, Québec, Canada

10 ²McGill Genome Centre, McGill University, Montréal, Québec, Canada

11 ³Quantitative Life Sciences, McGill University, Montreal, Québec, Canada

12 ⁴Department of Computational Biology, University of Lausanne, Lausanne, Switzerland

13 ⁵Montreal Heart Institute, Université de Montréal, Montreal, Québec, Canada

14 ⁶Programs in Metabolism and Medical & Population Genetics, The Broad Institute of MIT and Harvard,
15 Cambridge, MA, USA

16 ⁷Department of Human Genetics, McGill University, Montreal, Québec, Canada

17 ⁸Center for Genomic Medicine, Graduate School of Medicine, Kyoto University, Kyoto, Japan

18 ⁹Lady Davis Institute, Jewish General Hospital, McGill University, Montréal, Québec, Canada

19 ¹⁰Prime Sciences, Montréal, Québec, Canada

20 ¹¹Department of Epidemiology, Biostatistics and Occupational Health, McGill University, Montréal, Québec,
21 Canada

22 ¹²Department of Twin Research and Genetic Epidemiology, King's College London, London, United
23 Kingdom

24 ¹³Harvard Medical School, Boston, MA, USA

25 ¹⁴Department of Population Health Sciences, University of Wisconsin-Madison, Madison, WI, USA

26 ¹⁵Department of Biostatistics and Medical Informatics, University of Wisconsin-Madison, Madison, WI,
27 USA

28 ¹⁶Center for Genomic Science Innovation, University of Wisconsin-Madison, Madison, WI, USA

29 ¹⁷Center for Demography of Health and Aging, University of Wisconsin-Madison, Madison, WI, USA
30

31 ***Correspondence and equal contribution:**

32 Tianyuan Lu (tianyuan.lu@wisc.edu) and Satoshi Yoshiji (satoshi.yoshiji@mcgill.ca)

33 **Abstract**

34 Circulating proteins influence disease risk and are valuable drug targets. To enhance the
35 discovery of protein-phenotype associations and identify potential therapeutic targets across
36 diverse populations, we conducted proteome-phenome-wide Mendelian randomization in three
37 ancestries, followed by comprehensive sensitivity analyses. We tested the potential causal effects
38 of up to 2,265 unique proteins on a curated list of 355 distinct phenotypes, identifying 726,035
39 protein-phenotype pairs in European, 33,078 in African, and 115,352 in East Asian ancestries.
40 Notably, 119 proteins were instrumentable only in African ancestry and 17 proteins only in East
41 Asian ancestry due to allele frequency differences that are common in these ancestries but rare
42 in European ancestry. We identified 3,949, 56, and 325 unique protein-phenotype pairs in
43 European, African, and East Asian ancestries, respectively, and assessed their druggability using
44 multiple databases. We highlighted the causal role of IL1RL1 in inflammatory bowel diseases,
45 supported by multiple orthogonal lines of evidence. Taken together, this study underscores the
46 importance of multi-ancestry inclusion and offers a comprehensive atlas of protein-phenotype
47 associations across three ancestries, enhancing our understanding of proteins involved in disease
48 etiology and potential therapeutic targets. Results are available at the Common Metabolic
49 Diseases Knowledge Portal (https://broad.io/protein_mr_atlas).
50

51 Introduction

52 Circulating proteins play a major role in a multitude of biological pathways¹⁻³, are important
53 biomarkers for disease diagnosis, prognosis, and prevention⁴⁻⁶, and serve as valuable drug
54 targets⁷⁻¹⁰. Current high-throughput proteomics platforms measure thousands of circulating
55 plasma proteins. With measurements in large cohorts, recent studies have conducted genome-
56 wide association studies (GWAS) to evaluate genetic variants associated with the abundances of
57 thousands of proteins¹¹⁻¹⁴. We can leverage these proteomic GWAS to find causal proteins for
58 diseases and prioritize drug targets through Mendelian randomization (MR)^{15,16}. In this case, MR
59 uses genetic variants associated with variation in plasma protein levels (known as protein
60 quantitative trait loci, pQTLs) as instruments to measure the causal effect of an exposure (protein
61 abundance) on an outcome (a complex trait). This is shown to reduce confounding and reverse
62 causation biases affecting many epidemiological studies, provided that three key assumptions
63 are met: (1) the genetic variant is associated with the exposure, (2) there is no confounding of the
64 instrument-outcome association, and (3) the genetic variant influences the outcome solely
65 through the exposure.

66
67 Despite applications of proteogenomics in elucidating disease mechanisms and identifying
68 potential therapeutic targets¹⁷⁻²³, previous pQTL studies^{18,19} have been based on smaller sample
69 sizes and measured fewer proteins, assessed limited outcomes, and most importantly, have
70 predominantly focused on individuals of European ancestry. African ancestry proteomics cohorts
71 have emerged in recent years^{13,14,24}, yet existing studies have assessed a limited number of
72 outcomes and comparisons with other ancestries have also been limited¹⁹. Similarly, in East Asian
73 ancestries, few large-scale proteome-phenome wide MR studies exist^{25,26}, largely due to the lack
74 of publicly available pQTLs, despite the presence of existing East Asian ancestry biobanks
75 providing hundreds of publicly available GWAS outcomes^{27,28}.

76
77 The inclusion of multiple ancestries in a proteome-phenome wide atlas of associations can
78 potentially offer significant benefits. Diverse ancestry inclusion in MR leverages the natural
79 variations in genetic architecture present across populations, which allows analyses on otherwise
80 unseen genetic variation, increases in statistical power due to allele frequency increases, and
81 differentiation of causal effect magnitude across populations^{29,30}. Combined, this approach may
82 be able to identify a greater number of instrumentable proteins (i.e., proteins that can be tested
83 in MR), which may lead to an increase in discoveries. By leveraging insights obtained through
84 instrumentable proteins in one ancestry, the identified protein-phenotype associations could
85 contribute to our understanding of disease mechanisms, which may be generalizable across
86 different ancestries and potentially benefit all populations. For instance, PCSK9 loss-of-function
87 variants Y142X and C679X predispose individuals to naturally lower LDL cholesterol levels.
88 These mutations were found to be common in African Americans but rare in European
89 Americans³¹ and inspired the development of PCSK9 inhibitors mimicking these variants to
90 effectively reduce LDL cholesterol levels and risk of cardiovascular events^{32,33}. In addition to
91 providing insights into novel therapeutic targets, enhancing diversity in genomic studies is crucial
92 to ensure equitable health outcomes and address imbalances in health disparities across
93 populations³⁴.

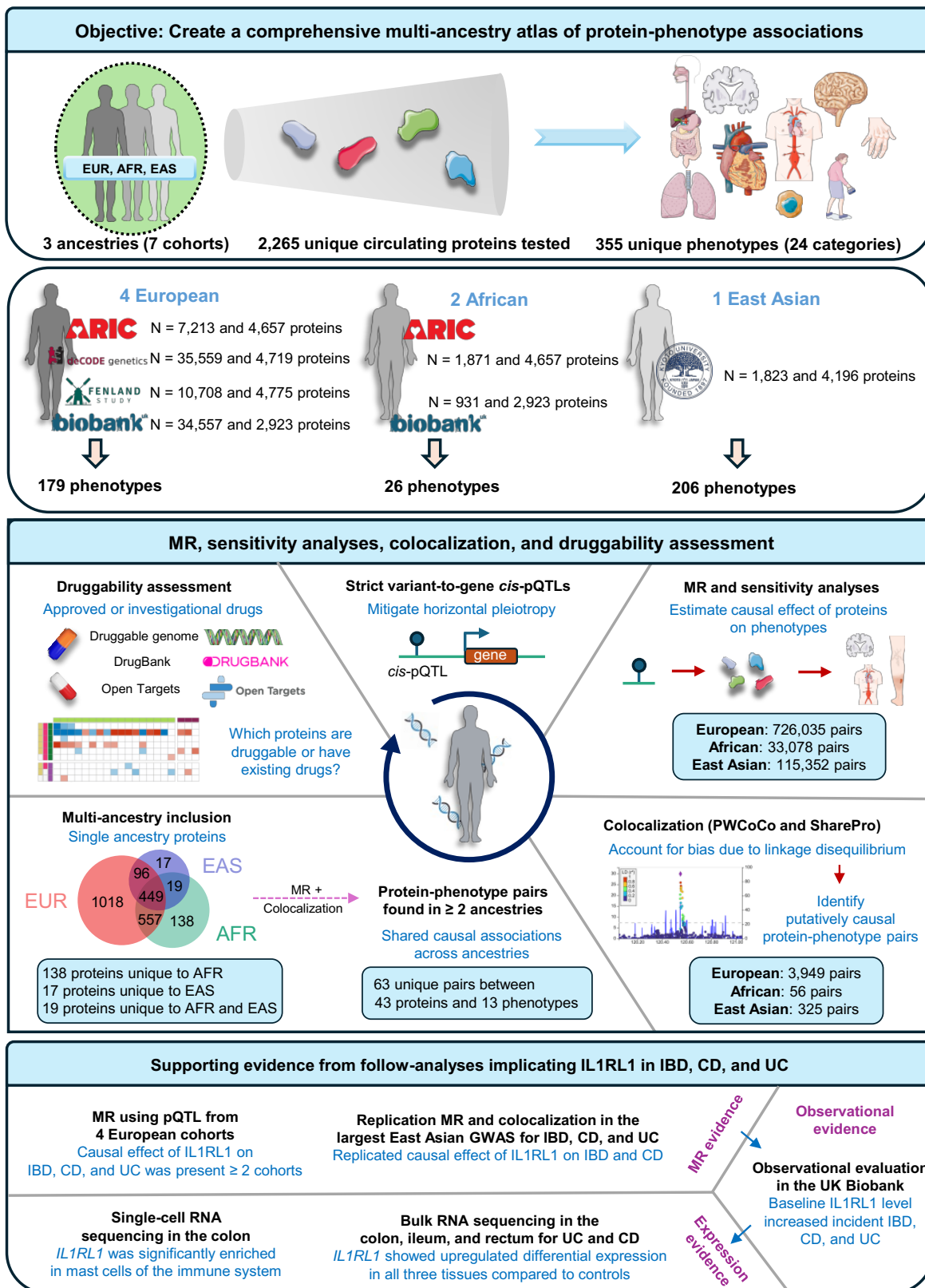
94
95 Here, we combined four of the largest European ancestry proteomics cohorts ($n =$ up to 35,559),
96 two of the largest African proteomics cohorts ($n =$ up to 1,871), and a new East Asian proteomics
97 cohort ($n =$ 1,823). We then performed MR and colocalization analyses on a curated list of the
98 most recent and largest ancestry-specific outcome GWAS to date for 179 European and 26
99 African ancestry outcomes, as well as 206 East Asian ancestry outcomes from Biobank Japan to
100 construct an atlas of protein-phenotype associations. We integrated our findings with multiple
101 drug databases to assess the druggability of the associations and highlighted novel targets.

102 Overall, our study supports the prioritization of thousands of protein-phenotype associations and
103 provides a comprehensive, updated resource for the community, significantly expanding our
104 understanding of these associations. Results are publicly available at the Common Metabolic
105 Diseases Knowledge Portal (https://broad.io/protein_mr_atlas).
106

107
108
109

Results

The overall study design is shown in Fig. 1.



110

111 **Figure 1. Study design.**

112 We assessed the causal role of 2,265 circulating plasma proteins across three ancestries (four
113 European, two African, and a new East Asian ancestry cohort) on up to 355 phenotypes/outcomes
114 with extensively curated GWAS in each ancestry. For European and African ancestry outcomes,
115 we collected the largest and most recent GWAS available as of February 2024 for 179 and 26
116 outcomes, respectively, while 206 GWAS from BioBank Japan were used for East Asian ancestry
117 outcomes. We implemented a unique approach for defining *cis*-pQTLs using a multi-step process
118 combining a strict *cis*-pQTL definition with Open Targets Genetics variant-to-gene score³⁵ filtering
119 to minimize risk of horizontal pleiotropy, which we term “strict variant-to-gene (V2G) *cis*-pQTLs”.
120 Then, we performed multi-ancestry proteome-wide MR and colocalization analyses using
121 PWCoCo^{18,36} and SharePro³⁷, a new colocalization method we developed, on the curated
122 phenotypes to identify causal protein-phenotype associations. Next, we overlapped prioritized
123 protein-phenotype pairs with drug databases such as the druggable genome³⁸, DrugBank³⁹, and
124 the Open Targets platform⁴⁰. Finally, as an illustrative example of the value of our atlas, we
125 pinpoint IL1RL1 and explore its role in inflammatory bowel disease using multiple lines of
126 evidence. EUR: European, AFR: African, EAS: East Asian; MR: Mendelian randomization; IBD:
127 Inflammatory bowel disease; CD: Crohn’s disease; UC: Ulcerative colitis.

128
129
130

131 **1. Genetic instrument selection for proteins**

132 We summarize the selected genetic instruments in **Supplementary Table 1**. Briefly, we used
133 proteomic GWAS from four European ancestry cohorts: ARIC (4,657 proteins measured in up to
134 7,213 individuals)¹³, deCODE (4,719 proteins measured in up to 35,559 individuals)¹², Fenland
135 (4,775 proteins measured in up to 10,708 individuals)¹¹, and UKB-PPP (2,923 proteins measured
136 in up to 34,557 individuals)¹⁴. For African ancestry, we analyzed proteomic GWAS from two
137 cohorts: ARIC (4657 proteins measured in up to 1,871 individuals)¹³ and UKB-PPP (2923 proteins
138 measured in up to 931 individuals)¹⁴. Additionally, we included a new East Asian ancestry cohort,
139 the Kyoto University Nagahama cohort which measured 4,196 proteins in up to 1,823 individuals.

140

141 **1.1. Unifying *cis*-pQTL across cohorts**

142 We re-defined *cis*-pQTLs across proteomics cohorts as pQTLs within 500 kb of the transcription
143 start site (TSS) of the protein-coding gene, with independence and significance defined with
144 linkage disequilibrium (LD) $r^2 < 0.001$ and $P < 5 \times 10^{-8}$, respectively. Independent pQTLs outside
145 the *cis*-region were labeled as *trans*-pQTLs. We analyzed *cis*-pQTLs because they are more likely
146 to have direct biological effects on the proteins of interest^{41,42}. We verified that newly defined *cis*-
147 pQTLs had high concordance within ancestries (**Supplementary Note 1A**).

148

149 **1.2. Identifying strict V2G *cis*-pQTLs**

150 We mitigated the risk of horizontal pleiotropy by using a unique approach to select genetic
151 instruments which we term strict V2G *cis*-pQTLs (**Supplementary Note 1B**). Strict V2G *cis*-
152 pQTLs are associated with a single protein-coding gene (“strict”) and have the strongest link to
153 the corresponding protein-coding gene based on the Open Targets Genetics V2G score, which
154 uses multiple sources of evidence to map variants to genes (“V2G”)³⁵ (**Extended Data Fig. 1** and
155 **Supplementary Tables 2–8**). We also assessed if these strict V2G *cis*-pQTLs were protein
156 altering variants (PAVs), as PAVs may affect protein structure and lead to bias in effect size
157 estimation¹. We found that only 70 of 7,399 (0.95%), 30 of 1,684 (1.8%), and 9 of 663 (1.4%)
158 strict V2G *cis*-pQTLs in European, African, and East Asian ancestries, respectively, were PAVs
159 or in high LD with PAVs of high impact. Notably, strict V2G *cis*-pQTLs were more enriched for *cis*-
160 eQTLs, indicating their role in local gene regulation impacting protein levels (**Extended Data Fig.**
161 **2a**). They had significantly larger effects on protein levels (**Extended Data Fig. 2b**) and were

162 significantly closer to the TSS of the corresponding protein-coding gene (**Extended Data Fig. 3**).
163 Hence, strict V2G selection of pQTLs limits the risks of violating MR assumptions (specifically no
164 horizontal pleiotropy) while still retaining adequate statistical power. Specifically, all proteins in
165 each cohort had F-statistics above 10, suggesting that the risk of weak instrument bias is limited⁴³
166 (**Supplementary Table 9**).

167 168 2. Multi-ancestry inclusion is important in instrumenting proteins and reveals population-specific 169 variants

170 Across the three ancestries, we were able to instrument 2,265 unique proteins with 449 of these
171 being shared across all three ancestries (**Fig. 2a**). Specifically, we instrumented 2,110 proteins in
172 European, 1,144 in African, and 581 in East Asian ancestries (see **Supplementary Note 1C** for
173 cohort level description and **Extended Data Fig. 4**). We identified 1,018 proteins that were unique
174 to individuals of European ancestry. Including African ancestries allowed for an additional 138
175 proteins, with 119 unique to African ancestry and 19 shared with East Asian ancestries. Including
176 an East Asian ancestry cohort allowed an additional 17 unique proteins (**Fig. 2a**). Altogether,
177 these findings underscore the value of including multiple ancestries in proteomic analyses.

178
179 Next, to better understand the unique proteins in non-European ancestries, we compared the
180 allele frequencies of their genetic instruments using gnomAD⁴⁴. Of the 130 genetic instruments
181 for the 119 proteins unique to African ancestries, 89 (68.5%) had a minor allele frequency (MAF)
182 below 0.01 in European ancestries (**Fig. 2b**). Similarly, for the 18 genetic instruments for the 17
183 proteins unique to East Asian ancestry, 13 (72.2%) had a MAF below 0.01 in European ancestry
184 (**Fig. 2c**). The majority (29, 63.0%) of the 46 unique genetic instruments for the 19 proteins
185 instrumentable by both African and East Asian but not by European ancestries, were rare (MAF
186 < 0.01) in European ancestry (**Fig. 2d**). These results suggest that populational allele frequency
187 differences allow for more proteins to be included in MR analyses. We refer to them as uniquely
188 instrumentable proteins.

189

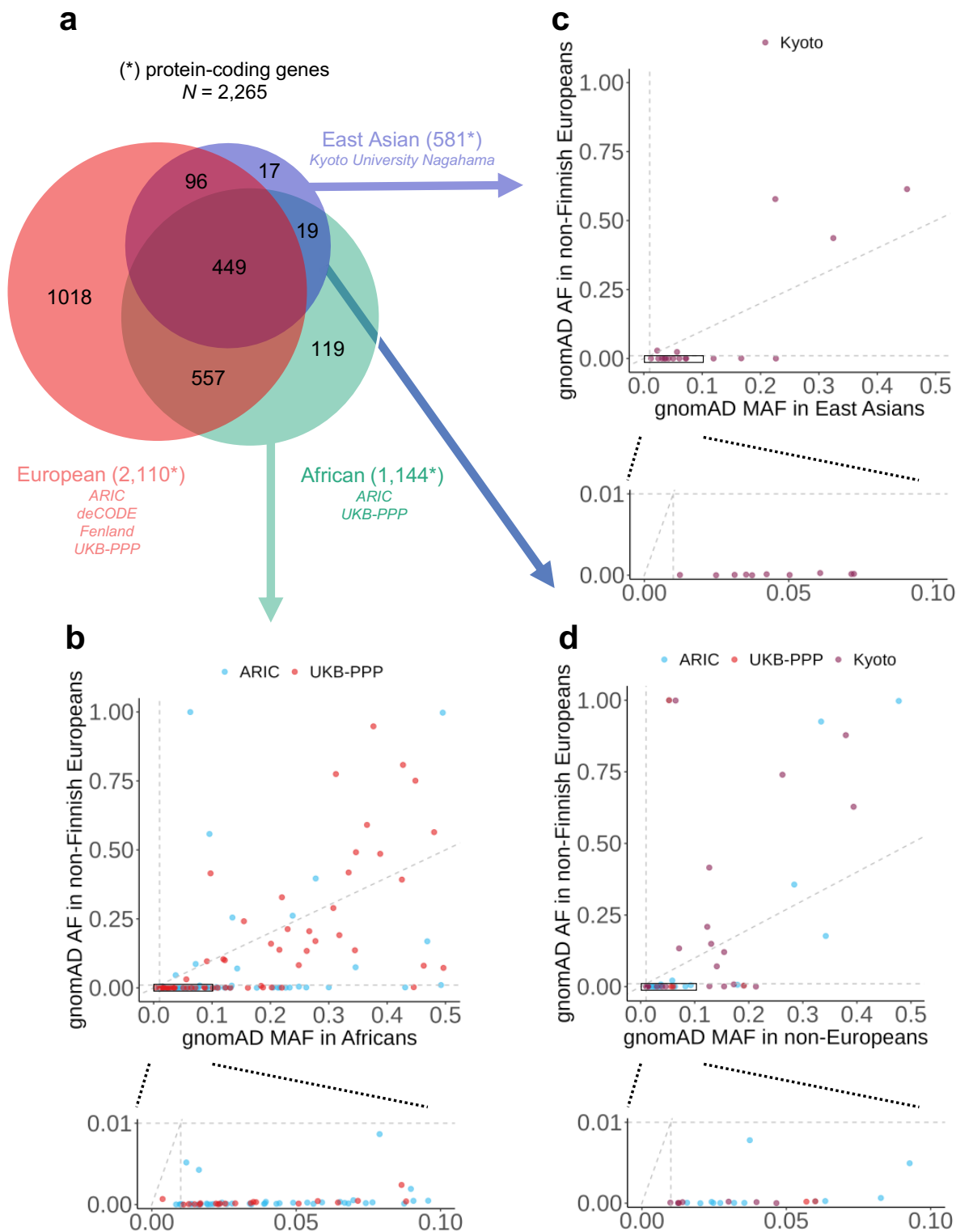


Figure 2. Cross ancestry comparison of overlapping instrumentable protein-coding genes.

(a) Overlapping instrumentable protein-coding genes across three ancestries. Protein-coding genes were quantified based on Ensembl gene IDs. Red: Unique protein-coding genes across four European ancestry proteomics cohorts; green: unique protein-coding genes across two African ancestry proteomics cohorts; blue: East Asian ancestry proteomics cohort protein-coding genes.

190
191
192
193
194
195
196

- 197 (b) gnomAD minor allele frequencies (MAF) of *cis*-pQTLs instrumenting the 119 proteins
198 uniquely instrumentable in African ancestry when plotted against corresponding gnomAD
199 non-Finnish European allele frequency (AF). The black box in the top plot is zoomed in
200 and shown in the bottom plot. Blue: ARIC African *cis*-pQTLs. Red: UKB-PPP African
201 ancestry cohort *cis*-pQTLs.
- 202 (c) gnomAD minor allele frequencies (MAF) of *cis*-pQTLs instrumenting the 17 proteins
203 uniquely instrumentable in East Asian ancestry when plotted against corresponding
204 gnomAD non-Finnish European AF. The black box in the top plot is zoomed in and shown
205 in the bottom plot. Purple: Kyoto University Nagahama East Asian ancestry cohort *cis*-
206 pQTLs.
- 207 (d) gnomAD MAF minor allele frequencies (MAF) of *cis*-pQTLs instrumenting the 19 proteins
208 common to African and East Asian but not European ancestries when plotted against
209 corresponding gnomAD non-Finnish AF. The black box in the top plot is zoomed in and
210 shown in the bottom plot. Blue: ARIC African *cis*-pQTLs. Red: UKB-PPP African *cis*-
211 pQTLs. Purple: Kyoto University Nagahama East Asian ancestry cohort *cis*-pQTLs.

212
213
214
215
216
217
218
219
220
221
222
223

3. Two-sample Mendelian randomization

We performed two-sample MR using strict V2G *cis*-pQTLs as instrumental variables to determine causal proteins implicated in human complex traits and diseases. Across three ancestries, we considered 355 unique outcomes (**Fig. 3a**) pertaining to 24 phenotype categories (**Fig. 3b**). These phenotypes/outcomes (as of February 2024) included 179 of the most up to date and largest phenotypic GWAS available for European ancestries (**Supplementary Table 10**), 26 of the largest available GWAS for African ancestries (**Supplementary Table 11**), and 206 from BioBank Japan for East Asian ancestries (**Supplementary Table 12**).

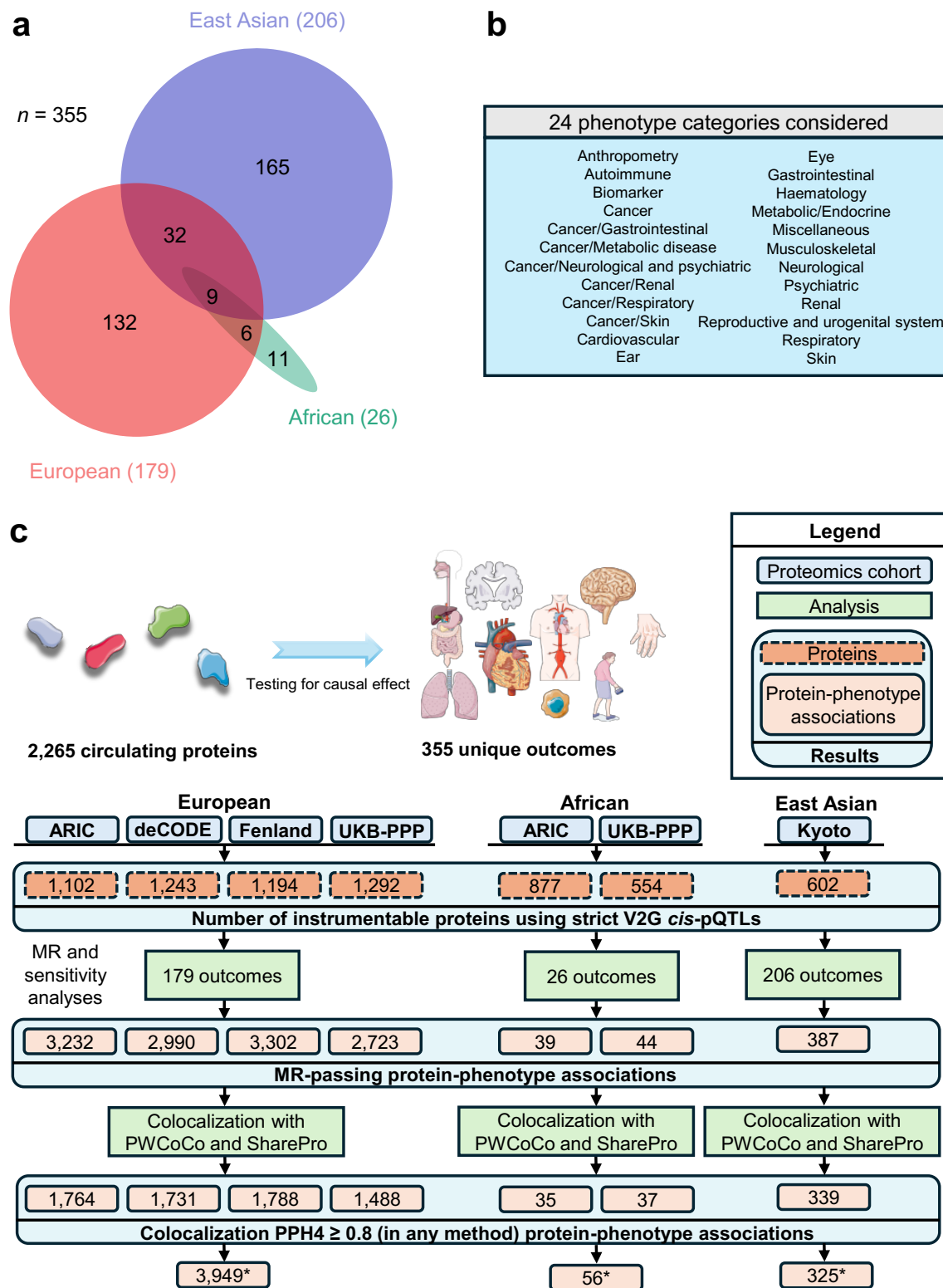


Figure 3. MR analyses to determine the effects of proteins on phenotypes.

(a) Curated GWAS phenotypes common between different ancestries. European (red), African (green), and East Asian (blue) ancestries.

224
225
226
227

- 228 (b) Phenotype categories for outcomes used in all three ancestries.
229 (c) Flowchart summary of MR and colocalization analyses to identify protein-phenotype
230 associations for each cohort.

231
232
233
234 We tested a total of 726,035 protein-phenotype pairs in European ancestries (173,748 for ARIC,
235 182,433 for deCODE, 180,018 for Fenland, and 189,836 for UKB-PPP), 33,078 in African
236 ancestries (20,442 for ARIC and 12,636 for UKB-PPP), and 115,352 in East Asian ancestries
237 (Kyoto University Nagahama cohort) (see **Data availability**). To control for false positives, we
238 applied a Benjamini-Hochberg-corrected P value (false discovery rate, FDR)⁴⁵ threshold of 0.05
239 (5%) per cohort in each ancestry¹⁹. We note that Bonferroni correction is overly stringent given
240 that (i) proteins are correlated with one another, and (ii) we tested the same protein-phenotype
241 associations across cohorts, making these tests not independent. Nevertheless, we also provide
242 the most stringent Bonferroni corrected associations in section 5. Results were further filtered
243 based on multiple sensitivity analyses robust to MR assumption violations and retained
244 associations are now termed "MR-passing". Assessment of sample overlap between European
245 ancestry GWAS outcomes that were based on the UK Biobank and proteomics from the European
246 ancestry UKB-PPP cohort was performed (**Supplementary Note 2**). Of the tested associations,
247 a total of 12,247 associations were considered MR-passing in European, 83 in African, and 387
248 in East Asian ancestries (**Supplementary Table 13**).

249 250 4. Colocalization analyses

251 MR results may be confounded by independent causal variants in LD^{46,47}. To guard against such
252 bias, for each MR-passing protein-phenotype pair, we performed colocalization analysis using
253 two methods, PWCoCo^{18,36} and SharePro³⁷, to verify that the protein abundance and the tested
254 outcome share the same genetic signals (**Fig. 3c**). An MR-passing protein-phenotype pair was
255 considered putatively causal if it was supported by at least one method with a posterior
256 colocalization probability (PP_{\max}) ≥ 0.8 . Across all cohorts and all three ancestries, 56.5% (7,182
257 out of 12,717) of MR-passing associations were supported by colocalization evidence
258 (**Supplementary Table 13**).

259 260 5. Putatively causal protein-phenotype associations

261 Upon MR, sensitivity analyses, and colocalization, we identified 3,949 unique putatively causal
262 protein-phenotype pairs in European (**Extended Data Fig. 5a** and **Supplementary Table 14**), 56
263 in African (**Extended Data Fig. 5b** and **Supplementary Table 15**), and 325 in East Asian
264 ancestries (**Extended Data Fig. 5c** and **Supplementary Table 16**). Here, we use protein to refer
265 to protein-coding genes to harmonize across SomaScan and Olink platforms. Results are also
266 hosted at https://broad.io/protein_mr_atlas. We described cohort level associations and proteins
267 implicated in a multitude of phenotypes in **Supplementary Notes 3 and 4**. Particularly, 1,617, 30,
268 and 135 unique associations in European, African, and East Asian ancestries further withstood
269 the Bonferroni correction accounting for the total number of tests across all cohorts and all
270 ancestries ($P < 0.05 / 874,465 = 5.7 \times 10^{-8}$), however, this threshold is likely overly conservative
271 due to many proteins being correlated with one another as well as non-independent tests from
272 the same protein-phenotypes associations being tested across cohorts (**Supplementary Tables**
273 **14 – 16**).

274
275 In European ancestries, the 3,949 significant unique protein-phenotype pairs identified in
276 European ancestries involved putatively causal effects between 995 proteins and 146 phenotypes,
277 of which only 56 (1.4%) showed discordant MR estimates in one of the tested cohorts
278 (**Supplementary Table 14**). These discrepancies could be attributed to population differences or

279 variations in proteomic assays, such as differential effects from SomaScan aptamers targeting
280 different domains compared to Olink assays. Of the 3,893 remaining putatively causal European
281 ancestry pairs between 991 proteins and 146 outcomes, 1,692 (43.5%) of the identified putatively
282 causal associations were from 452 proteins uniquely instrumentable by European ancestries.
283 Further, 3,853 (99.0%) associations have not been previously reported by earlier proteome-
284 phenome wide MR studies from Zheng et al.¹⁸ and Zhao et al.¹⁹.

285

286 *5.1. Cardiovascular and autoimmune diseases*

287 We demonstrate the highly interconnected nature between proteins and outcomes by highlighting
288 cardiovascular (**Fig. 4a** and **Supplementary Note 5A**) and autoimmune phenotypes (**Fig. 4b**) in
289 European ancestries given their significant impact on health. Cardiovascular outcomes were
290 influenced by up to 103 proteins (median: 7) while some proteins influenced up to 8 cardiovascular
291 outcomes (median: 1) (**Fig. 4a**). For instance, we found that an s.d. increase in genetically
292 predicted ULK3 levels increases systolic and diastolic blood pressure, pulse pressure, and
293 hypertension. ULK3 is a nuclear kinase which may contribute to vascular disease by mediating
294 autophagy dysregulation⁴⁸. In concordance, a recent study showed that functional splicing effects
295 of ULK3 can contribute to coronary artery disease (CAD)⁴⁹ suggesting effective modulation of
296 ULK3 may be beneficial for reducing cardiovascular risk.

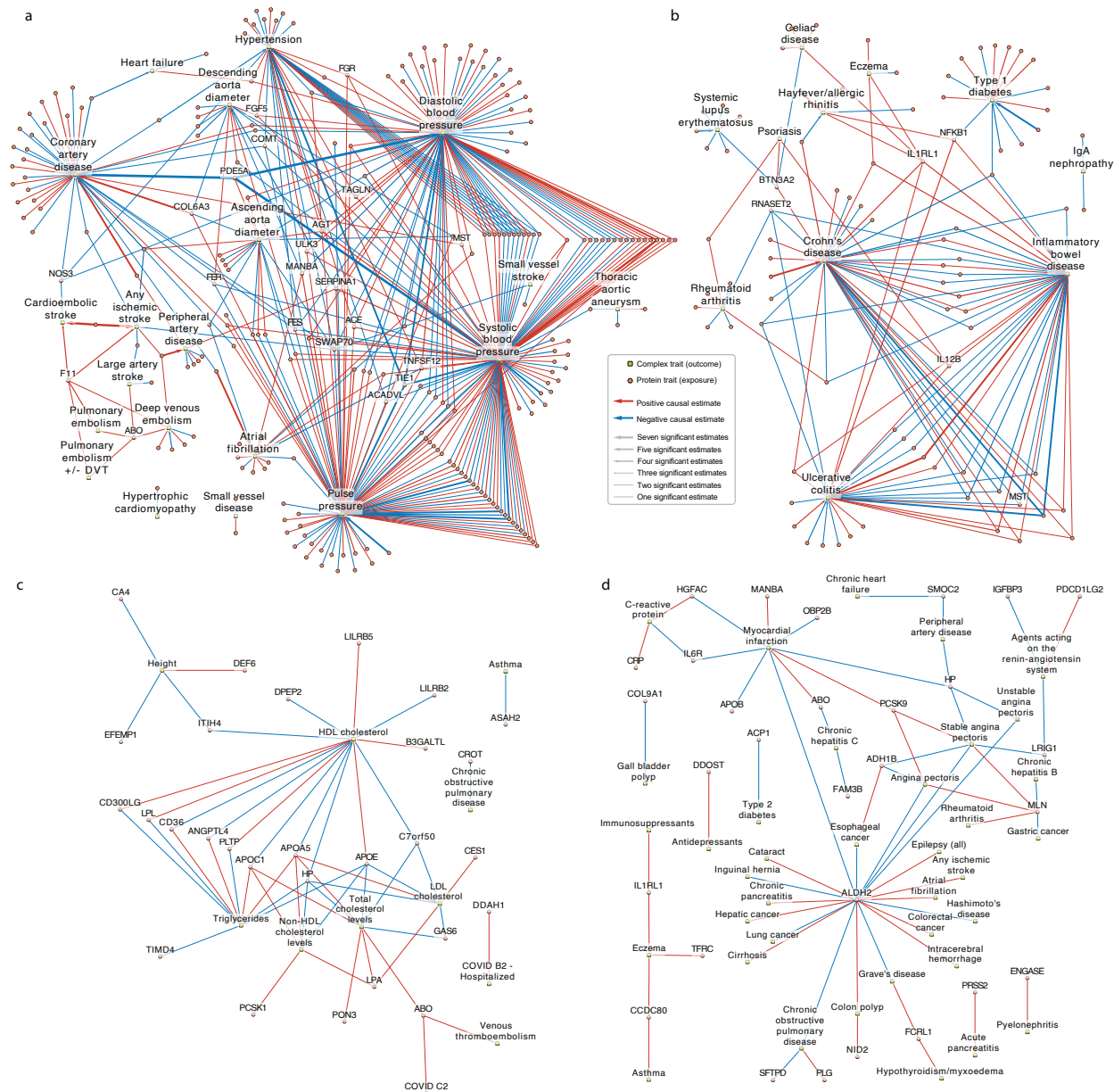
297

298 Similarly, we found high interconnectedness between autoimmune phenotypes and proteins (**Fig.**
299 **4b**). Autoimmune phenotypes were influenced by a median of 7 proteins; the highest number of
300 associations were for Crohn's disease (CD) (39 proteins), inflammatory bowel disease (IBD) (35
301 proteins), and ulcerative colitis (UC) (28 proteins). Proteins, on the other hand, influenced a
302 median of 2 autoimmune phenotypes. IL1RL1 and IL12B influenced the largest number of
303 outcomes (6 and 4 outcomes, respectively) (**Fig. 4b**) with both increasing risk of IBD, CD, and
304 UC. IL12B is targeted by a commercially available drug ustekinumab for CD⁵⁰; however, there are
305 currently no approved drugs targeting IL1RL1, although there has been increasing interest in
306 modulating IL1RL1 for treating various conditions^{51,52}. For example, tozorakimab targets IL-33,
307 the interleukin that binds IL1RL1 (ST2)⁵³ and anakinra targets IL-1⁵⁴, a closely related interleukin.

308

309 Other potentially novel findings involving other disease categories in European ancestries are
310 highlighted in **Supplementary Note 5B**.

311



312
313
314
315
316
317
318
319
320
321
322
323
324
325
326

Figure 4. Protein-phenotype network plots.

Red arrows indicate a positive causal estimate of the protein on the phenotype while blue arrows indicate a negative causal estimate of the protein on the phenotype.

(a) Significant estimates between proteins (orange circles) and cardiovascular traits (green rectangles) both derived from European ancestry individuals. All cardiovascular traits are named, as well as the protein traits that have a significant effect on 4 or more cardiovascular traits. Arrow thickness representing number of significant estimates indicates how often a protein measurement has a causal effect on the outcome trait. The maximum number of significant estimates is 7 which is larger than the total number of European ancestry proteomics studies, 4, due to the presence of more than one SomaScan aptamer for that protein. For simplicity, we only depict protein-phenotype pairs in which all European ancestry cohorts showed concordant direction of effect estimates.

(b) Significant estimates between proteins (orange circles) and autoimmune traits (green rectangles) both derived from European ancestry individuals. All autoimmune traits are

327 named, as well as the protein traits that have a significant effect on 4 or more autoimmune
328 traits. Arrow thickness representing number of significant estimates indicates how often a
329 protein measurement has a causal effect on the outcome trait. For simplicity, we only
330 depict protein-phenotype pairs in which all European ancestry cohorts showed concordant
331 direction of effect estimates.

332 (c) Significant estimates between proteins (orange circles) and all traits (green rectangles)
333 both derived from African ancestry individuals. All arrows are the same thickness to
334 indicate support of the association in a single study.

335 (d) Significant estimates between proteins (orange circles) and binary traits (green
336 rectangles) both derived from East Asian ancestry individuals. All arrows are the same
337 thickness and indicate support of the association in a single study.

338
339
340

341 *5.2. Protein-phenotype associations in African and East Asian ancestries*

342 In African ancestries, we identified 56 unique protein-phenotype associations involving 28
343 proteins and 11 phenotypes (**Fig. 4c** and **Supplementary Table 15**). Of these 56 pairs, 55
344 (98.2%) have not been previously reported by earlier proteome-phenome wide MR studies in
345 African ancestries¹⁹. Notably, 11 (19.6%) protein-phenotype pairs involving four proteins, APOE,
346 C7orf50, CD300LG, and PON3, were uniquely instrumentable in African ancestries (**Extended
347 Data Fig. 6a**). For instance, increased PON3 levels was associated with increased total
348 cholesterol ($\beta_{\text{UKB-PPP}} = 0.03$, 95% CI = 0.02–0.05, $P = 1.1 \times 10^{-5}$, $\text{PP}_{\text{max}} = 0.95$). *PON3* is highly
349 expressed in the liver and previously implicated in cholesterol metabolism^{55,56} and atherosclerosis
350 progression. This is notable as *PON3* was not instrumentable in European ancestries, thus,
351 African ancestries are uniquely suitable to identify biologically plausible protein-phenotype
352 associations.

353
354 Furthermore, the Million Veteran Program⁵⁷ recently released summary statistics for additional
355 traits in up to 635,969 individuals. Using this resource, we tested the causal effect of the 119
356 proteins uniquely instrumentable in African ancestries on cardiovascular and autoimmune-related
357 binary outcomes. Using the African ARIC proteomics cohort, we identified 7 associations with
358 cardiovascular outcomes and no associations with autoimmune-related outcomes
359 (**Supplementary Note 5C**). Notably, increased PCYOX1 levels were associated with a reduced
360 risk of coronary atherosclerosis, atrial fibrillation, and flutter, indicating its protective effect.
361 PCYOX1 plays a role in oxidative stress and lipid metabolism and has been implicated in
362 atherosclerosis in rodent studies⁵⁸, supporting our findings. This suggests that as more outcomes
363 with larger sample size, particularly binary disease outcomes, become available in African
364 ancestries, we can better leverage uniquely instrumentable proteins to uncover additional protein-
365 disease associations.

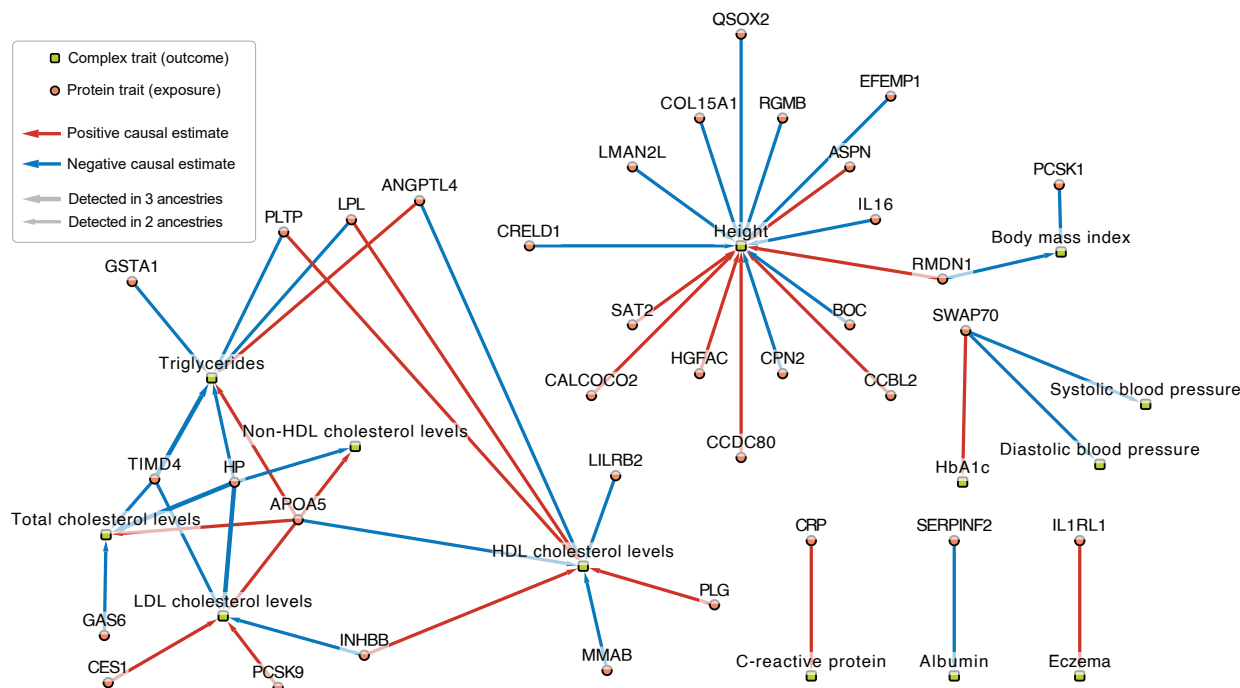
366
367 In East Asian ancestries, 339 putatively causal associations were identified with 325 unique
368 protein-phenotype pairs involving 110 proteins and 86 phenotypes (**Fig. 4d** and **Supplementary
369 Table 16**). Among them, increased SMOC2 level was associated with decreased risk of peripheral
370 artery disease (PAD) (OR = 0.82, 95% CI = 0.74–0.90, $P = 5.5 \times 10^{-5}$, $\text{PP}_{\text{max}} = 0.97$). *SMOC2* is
371 highly expressed in arteries and plays roles in endothelial cell proliferation, angiogenesis, and
372 matrix assembly⁵⁹. Notably, in European ancestries, increased SMOC2 was associated with
373 decreased pulse pressure, implicating favorable cardiovascular effects across ancestries.

374
375 We also found 8 proteins which were only instrumentable in East Asian ancestry due to lack of
376 genome-wide significant *cis*-pQTLs in other ancestries or stringent strict V2G instrument selection
377 (**Supplementary Note 5D**). These 8 proteins were ALDH2, ANXA7, APOA1, DDOST, GSS,

378 PLA2G7, PRSS2, and UGT1A1 which together accounted for 67 (20.6%) protein-phenotype
 379 associations (**Extended Data Fig. 6b** and **Supplementary Note 5D**). For instance, increased
 380 PRSS2 levels in East Asian ancestries was associated with an OR of 2.05 for acute pancreatitis
 381 (95% CI: 1.42–2.98, $P = 1.43 \times 10^{-4}$, $PP_{\max} = 0.95$) which has been previously validated in
 382 European only proteome-wide analyses⁶⁰ suggesting concordant effects across ancestries.
 383

384 6. Concordant effects across ancestries

385 We evaluated the direction of effect for protein-phenotype associations that passed MR and
 386 colocalization analyses across ancestries since concordance across ancestries may strengthen
 387 the evidence of broader applicability of therapeutic targets. We found 186 total protein-
 388 phenotype/outcome pairs with 63 unique pairs between 43 proteins and 13 outcomes
 389 (**Supplementary Table 17** and **Fig. 5**). Among these, 51 pairs (81.0%) had concordant effects
 390 across ancestries, while 12 pairs (19.0%) had inconsistent effects (**Supplementary Figure 3** and
 391 **Supplementary Note 6**). Notable concordant associations included PCSK9 and LDL cholesterol
 392 in European and East Asian ancestries, and haptoglobin (HP), which binds free hemoglobin to
 393 prevent oxidative damage, with LDL cholesterol and total cholesterol across all three ancestries.
 394 Angiotensin-related protein 4 (ANGPTL4) was negatively associated with HDL cholesterol and
 395 positively with triglycerides in European and African ancestries, while lipoprotein-lipase (LPL)
 396 showed opposite associations in these ancestries. ANGPTL4 has been shown to act as a local
 397 inhibitor of LPL⁶¹ which serves as the rate-limiting enzyme in the degradation of triglycerides⁶²,
 398 concordant with our findings. While no approved drugs exist for ANGPTL4, inhibition of a closely
 399 related protein ANGPTL3 through an RNA interference therapy zodasiran is currently undergoing
 400 clinical trials for cholesterol lowering⁶³. Thus, many of these biological effects were validated in
 401 our multi-ancestry analyses. We note that while concordant effects across ancestries provide
 402 strong evidence of support, discordant effects in MR do not automatically indicate biologically
 403 discordant effects across ancestries, which could be due to epitope-binding effects or other
 404 technical variations⁶⁴.



405
 406

407 **Figure 5. Multi-ancestry network plot for protein-phenotype pairs present in two or more**
408 **ancestries.**

409 All estimates shown had evidence in European ancestry and at least one other ancestry (African
410 or East Asian ancestry). Significant estimates between proteins (orange circles) and traits (green
411 rectangles). Arrow thickness indicates the number of ancestries in which a protein measurement
412 has a causal effect on the phenotype. For simplicity, we only depict estimates when cohorts within
413 the same ancestry and across different ancestries showed concordant direction of effect
414 estimates. Red arrows indicate a positive causal estimate of the protein on the phenotype while
415 blue arrows indicate a negative causal estimate of the protein on the phenotype.

416
417
418
419 **7. Druggability**

420 *7.1. Druggability of the instrumentable protein-coding genes*

421 Across all ancestries, between 60% to 67% of instrumentable protein-coding genes overlapped
422 with the druggable genome³⁸, which classifies genes into Tier 1, 2, or 3 according to druggability,
423 and between 20.5% and 23.6% overlapped with Tiers 1 and 2 (**Supplementary Table 18** and
424 **Supplementary Note 7A**). Druggability tiers for instrumentable proteins are in **Supplementary**
425 **Tables 19–25**.

426
427 Next, we incorporated the druggable genome³⁸, DrugBank³⁹, and Open Targets Platform⁴⁰ to
428 determine which instrumentable proteins overlapped at least one database. Proteins overlapping
429 with DrugBank³⁹ had approved or investigational drugs available while those overlapping Open
430 Targets have information on their clinical development phase and status of protein-drug-disease
431 combinations. Cross-ancestry comparison stratified by proteomics platform for instrumentable
432 proteins overlapping at least one database shows that in SomaScan v4, African ancestry adds 68
433 additional targets beyond European ancestry cohorts (**Extended Data Fig. 7a**), while East Asian
434 ancestry contributes 34 more targets (**Extended Data Fig. 7b**). In Olink Explore 3072, including
435 African ancestry presents 62 additional targets (**Extended Data Fig. 7c**). These findings suggest
436 that data from African and East Asian ancestries could enhance drug development by offering
437 more potential therapeutic targets.

438
439 *7.2. Druggability of protein-phenotype pairs by integrating the druggable genome, DrugBank,*
440 *and Open Targets Platform*

441 Across three ancestries, among the 1,037 number of protein-coding genes that have at least one
442 protein-phenotype association, 669 (64.5%) were present in at least one database. Specifically,
443 579 (55.8%) protein-coding genes overlapped with the druggable genome³⁸, 350 (33.8%) had
444 approved or investigational drugs in DrugBank³⁹, and 191 (18.4%) overlapped with the Open
445 Targets Platform⁴⁰ (**Supplementary Table 26**). Notably 32 (3.1%) were unique to non-Europeans.
446 This highlights that multi-ancestry inclusion can expand the list of actionable druggable
447 associations. Overlap with the druggable genome and DrugBank stratified by ancestry is
448 presented in **Supplementary Note 7B**.

449
450 We found that higher levels of MANBA, a Tier 2 target, increased risk of atrial fibrillation in
451 European ancestry (**Fig. 6a**) and myocardial infarction in East Asian ancestry (**Fig. 6b**). Currently
452 no drugs exist for MANBA but its role in lysosomal metabolism suggests that modulating its activity
453 could have therapeutic potential. Further, increased ANGPTL4, a Tier 3 target, leads to increased
454 triglycerides and decreased HDL cholesterol levels in African ancestries (**Fig. 6c**) and increased
455 CAD risk in European ancestries (**Supplementary Note 7C**) supporting its potential as a
456 therapeutic target. Notably, we found that increased STAT3, a Tier 1 target, increased risk of IBD

457 and its subtypes, CD, and UC (**Fig. 6d**). Danvatirsen, a STAT-3 mRNA 3'UTR antisense inhibitor
458 has been undergoing phase 1 and 2 clinical trials for multiple cancer types and may be potentially
459 repurposed for IBD. Currently, astegolimab, an inhibitor of IL1RL1, a Tier 3 target, has completed
460 phase 2 trials for eczema and asthma; in our study, we find genetic support where increased
461 IL1RL1 increased risk of eczema in East Asian ancestry (**Fig. 6e**) and was concordant in
462 European ancestries (**Supplementary Table 17**). Druggability visualization for remaining
463 diseases for European and East Asian ancestries are provided in **Supplementary Note 7C**.
464

468 Legend information:

469 Each cell displays a putatively causal protein-phenotype association. Cell color displays the MR
470 effect estimate based on Z score averaged across cohorts capped at -10 to +10 with red showing
471 a positive Z score indicating a positive MR effect of the protein (displayed as the gene name) on
472 the phenotype and blue showing a negative Z score indicating a negative MR effect of the protein
473 on the phenotype. For simplicity, in European ancestries, we only display protein-phenotypes with
474 consistent effect across European cohorts.

475 The y-axis shows the three drug databases. DrugBank (yellow square): DrugBank³⁹ shows
476 whether the protein has an available drug in the database. Open Targets (pink square): Open
477 Targets Platform⁴⁰ shows whether the protein has available clinical trial information. Druggability:
478 The druggable genome from Finan et al.³⁸ is shown for Tiers 1 (dark green, representing direct
479 targets of approved small molecules and biotherapeutic drugs), Tier 2 (dark purple, representing
480 proteins closely related to approved drug targets or which have associated drug-like compounds),
481 Tier 3 (light purple, representing secreted or extracellular proteins, those distantly related to
482 approved drug targets, and members of important druggable gene families not covered in Tier 1
483 or Tier 2), and Unclassified (gray, all other proteins not in Tiers 1 to 3). Proteins on the y-axis
484 within each tier are sorted based on the number of supported databases.

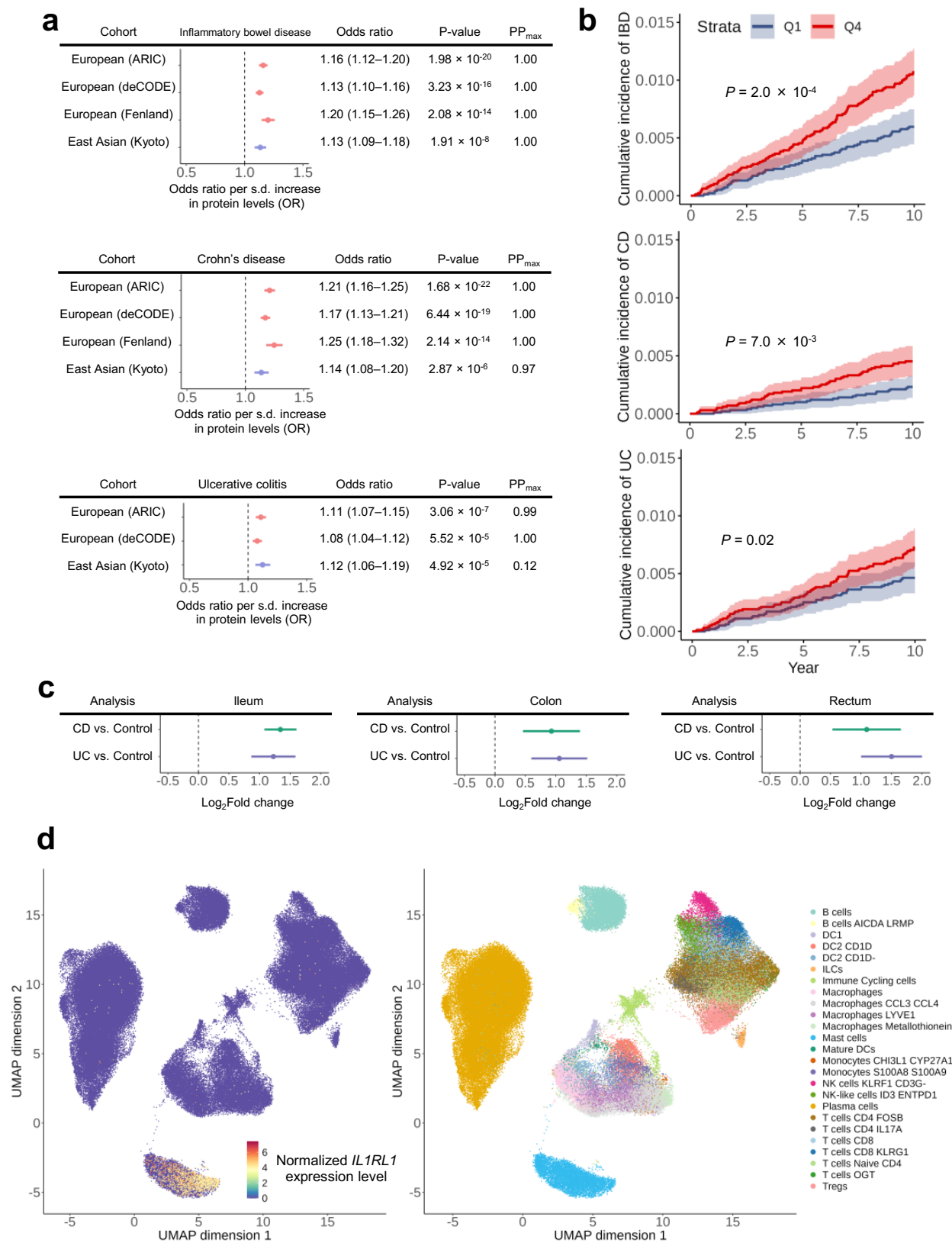
- 485 (a) European ancestry putatively causal protein-phenotype pairs stratified to Tier 1 and Tier
486 2 druggable proteins and cardiovascular phenotypes.
- 487 (b) East Asian ancestry putatively causal protein-phenotype pairs stratified to Tier 1 and Tier
488 2 druggable proteins and cardiovascular phenotypes.
- 489 (c) All of the African ancestry putatively causal protein-phenotype pairs with no druggability
490 stratification.
- 491 (d) European ancestry putatively causal protein-phenotype pairs stratified to Tier 1 and Tier
492 2 druggable proteins and autoimmune phenotypes.
- 493 (e) East Asian ancestry putatively causal protein-phenotype pairs stratified to autoimmune
494 phenotypes.

495
496
497

498 8. Converging evidence of the causal effect of IL1RL1 on IBD

499 Upon further stringent filtering to find protein-phenotype pairs with strong evidence (see **Methods**),
500 we found that increased IL1RL1 levels was associated with increased risk of IBD, CD, and UC in
501 European ancestries across three cohorts for IBD and CD and two cohorts for UC with consistent
502 directions, which we validated using the largest available East Asian ancestry GWAS for IBD
503 (14,393 cases and 15,456 controls), CD (7,372 cases and 15,456 controls), and UC (6,862 cases
504 and 15,456 controls) from Liu et al.⁶⁵ (**Fig. 7a**). In African ancestries, the number of cases were
505 limited in the largest publicly available GWAS for IBD (1,285 cases and 119,314 controls)⁵⁷ and
506 UC (857 cases and 119,909 controls)⁵⁷, thus estimates were not significant likely due to
507 insufficient power.

508



509
510

Figure 7. *IL1RL1* in IBD, CD, and UC.

- 511 a) MR for the effect of *IL1RL1* and IBD (top), CD (middle), and UC (bottom) in European and
512 East Asian ancestries. PP_{\max} is the maximum colocalization posterior probability between
513 PWCoCo and SharePro.
514 b) Kaplan Meier estimates for cumulative incident of IBD (top), CD (middle), and UC (bottom)
515 by baseline *IL1RL1* level quantiles in the UK Biobank. P values were computed using the
516 log-rank test.
517 c) Bulk RNA sequencing of *IL1RL1* in the ileum (left), colon (middle), and rectum (right).
518 d) Single-cell RNA sequencing analyses of *IL1RL1*. *IL1RL1* expression patterns showing
519 720,633 cells collected from the terminal ileum and colon of 71 donors with different levels
520 of inflammation. Single-cell transcriptomic data was obtained from Kong et al.⁶⁶ (SCP1884
521 <https://singlecell.broadinstitute.org/>).
522
523
524

525 To triangulate the evidence, we performed supplementary observational analysis in the UK
526 Biobank using Cox proportional hazards models. We adjusted for age, sex, recruitment center,
527 Olink measurement batch, Olink processing time, and the first 10 genetic principal components.
528 Notably, none of the genetic principal components were significant, suggesting that the
529 association is not specific to ancestry. Over 10 years of follow-up, a one s.d. increase in *IL1RL1*
530 was associated with elevated risk of IBD (hazard ratio, HR = 1.18; 95% CI: 1.05–1.33; $P = 6.6 \times$
531 10^{-3}), CD (HR = 1.21; 95% CI: 1.00–1.47; $P = 0.047$), and UC (HR = 1.15; 95% CI: 1.00–1.33; P
532 = 0.048), consistent with MR findings (**Supplementary Table 27**). Kaplan-Meier estimates for
533 cumulative incidence of disease stratified by baseline *IL1RL1* level (lowest 25% versus highest
534 25% in the UK Biobank population) also showed differences in IBD (log-rank test $P = 2.0 \times 10^{-4}$),
535 CD (log-rank test $P = 7.0 \times 10^{-3}$), and UC (log-rank test $P = 0.02$) (**Fig. 7b**). We also performed
536 an alternative, less stringent filter and prioritized proteins involved in CAD and type 2 diabetes
537 which we provide in **Supplementary Note 8**.
538

539 8.1. *IL1RL1* expression analyses

540 To further assess the role of *IL1RL1* in IBD, we used the IBD Transcriptome and
541 Metatranscriptome Meta-Analysis (IBD TaMMA) platform⁶⁷ to compare expression of *IL1RL1*
542 transcripts between IBD patients and healthy controls in the ileum, colon, and rectum. We found
543 significantly higher *IL1RL1* gene expression in all three tissues (**Fig. 7c**), suggesting that
544 increased *IL1RL1* expression is a consistent feature of IBD regardless of the specific location
545 within the gastrointestinal tract.
546

547 To gain further insights into the role of *IL1RL1* in IBD, CD and UC, we analyzed single-cell *IL1RL1*
548 expression in 720,633 cells from the terminal ileum and colon of 71 participants with different
549 levels of inflammation status from Kong et al.⁶⁶ (SCP1884 <https://singlecell.broadinstitute.org/>). In
550 single-cell RNA sequencing, *IL1RL1* showed significant enrichment in mast cells compared to 24
551 other cell types (permutation $P < 2.0 \times 10^{-4}$) (**Fig. 7d**). Mast cells, key players in allergic reactions
552 and inflammation and a key cell type involved in the pathogenesis of IBD^{68,69}, may contribute to
553 chronic IBD by releasing inflammatory mediators like histamine and cytokines when activated by
554 *IL1RL1* in inflamed tissues. These findings align with our MR analyses showing that increased
555 *IL1RL1* leads to increased risk of IBD, CD and UC.
556

557 Discussion

558 In this study, we conducted comprehensive multi-ancestry proteome-phenome analyses across
559 three ancestries. Using seven large proteomics cohorts including European, African, and East
560 Asian ancestries, we analyzed 355 complex traits or diseases, and identified 3,949, 56, and 325
561 putative causal effects of protein abundance on diseases and traits, respectively. By integrating
562 data from druggable genomes and drug databases, we prioritized potential protein targets for
563 drug development. Our findings offer a comprehensive atlas of protein-phenotype associations
564 and an evidence-based resource to support drug discovery and development, expand insight into
565 disease, and highlight potential targets for therapeutic intervention.

566
567 Our study provides an updated map to earlier phenome-wide MR studies of the human plasma
568 proteome on complex diseases which were either limited to European ancestries¹⁸ or considered
569 only a few diseases in European and African ancestries¹⁹. The significance of incorporating
570 multiple ancestries is underscored by our identification of several proteins that are uniquely
571 instrumentable by each ancestry due to allele frequency differences. Specifically, we
572 instrumented an additional 119 proteins exclusively in African ancestry, 17 in East Asian ancestry,
573 and 19 shared between African and East Asian ancestries. Moreover, the finding that a significant
574 proportion of population-specific genetic variants—68.5% in African and 72.2% in East Asian—
575 have a MAF below 0.01 in European ancestries highlights the potential for missed genetic
576 discoveries when studies focus on a single ancestry. Research on the genetic architecture across
577 different ancestries reveals both commonalities and differences, influenced by evolutionary
578 history, genetic diversity, and population-specific factors^{26,30}. Thus, by including diverse African
579 and East Asian ancestries in proteomic analyses, we were able to instrument more proteins by
580 leveraging common genetic variants in these underrepresented populations which were mostly
581 rare in European ancestries, enhancing the potential for novel discoveries and exemplifying the
582 value of including non-European individuals for comprehensive and inclusive proteomic and
583 genetic analyses.

584
585 The inclusion of African and East Asian ancestries allowed discovery of protein-phenotype
586 associations. We emphasize that these findings were attributable to uniquely instrumentable
587 proteins in each ancestry and do not necessarily indicate ancestry-specific biological mechanisms.

588
589 As an illustrative example of the value of our atlas, we found that increased circulating
590 abundances of IL1RL1 was causal for IBD, CD, and UC in European and East Asian ancestries,
591 which was supported by observational analyses and gene expression analyses. IL1RL1 could be
592 a promising therapeutic approach for IBD, potentially reducing mast cell-driven inflammation.
593 Potential drugs targeting IL1RL1 include astegolimab which has completed phase 2 trials for
594 eczema and asthma, tozorakimab which neutralizes IL-33, the interleukin that binds IL1RL1 (ST2),
595 and anakinra which targets IL-1, a closely related interleukin. However, further research is
596 required to assess the safety and efficacy of potential IL1RL1 inhibition. Many such findings may
597 exist, and this atlas may be used as a tool to facilitate the selection of targets during primary or
598 pre-clinical drug development, exploring drug repurposing opportunities, and improve
599 understanding of proteins implicated in complex traits and diseases.

600
601 Our study has several key strengths. We curated GWAS for a wide range of complex traits and
602 diseases, decreasing the overlap and redundancy and increasing the power for discovery in MR.
603 Second, our study included diverse proteomics cohorts, including African ancestry and a new
604 East Asian ancestry cohort, the Kyoto University Nagahama cohort. This latter cohort, which used
605 the SomaScan v4 platform, is the largest to date aside from the China Kadoorie Biobank^{25,26}.
606 Further, our study combined both ARIC SomaScan and UKB-PPP Olink African proteomics
607 cohorts at a phenome-wide scale and to include three ancestries. Notably, we identified uniquely

608 instrumentable proteins in African and East Asian ancestries that were not found in European
609 ancestries, highlighting the value of including cohorts from diverse ancestral backgrounds. Third,
610 we performed extensive stringent filtering on genetic instruments with strict V2G criteria. Fourth,
611 we harnessed novel state-of-the-art colocalization methods to reduce the risk of confounding from
612 LD while increasing the statistical power to support more protein-phenotype associations with
613 colocalization evidence³⁷.

614
615 This study has several limitations. First, while two separate proteomics cohorts were included for
616 African ancestries, the number of outcomes considered was still limited. Additionally, African
617 ancestry phenotypes were curated from various cohorts with potentially finer genetic architecture
618 differences than controlled for by using continental ancestries, thereby potentially biasing our
619 analyses. Second, differences in measurement units make direct comparison of MR effect size
620 estimates for continuous outcomes difficult. Nevertheless, direction of effect should be robust to
621 this limitation. Third, while we reduced the risk of horizontal pleiotropy by using strict V2G *cis*-
622 pQTLs, this resulted in many proteins being instrumented by a single *cis*-pQTL, limiting the ability
623 to perform MR sensitivity analyses. Nonetheless, we used robust colocalization methods to
624 mitigate risk of reporting false positives. Fourth, although we used assays measuring nearly 5,000
625 proteins from SomaScan and 3,000 proteins from Olink, coverage is still limited with regard to the
626 entire proteome. Lastly, while we analyzed three diverse ancestries, the sample sizes for both
627 proteomic GWAS and outcome GWAS were much larger for European ancestry, leading to
628 differences in the number of associations. Greater coverage of proteins and larger sample sizes
629 in non-European ancestries are needed.

630
631 In conclusion, through integrative multi-ancestry plasma proteome-phenome MR and extensive
632 sensitivity analyses, we provided a comprehensive atlas of protein-phenotype associations
633 across three ancestries and highlighted the value of multi-ancestry inclusion, as illustrated by
634 uniquely instrumentable proteins in non-European ancestries. This study serves as a valuable
635 resource for understanding disease mechanisms and prioritizing potential new targets.
636

637 **Methods**

638 **1. Proteomics cohorts**

639 We analyzed proteomics cohorts from three ancestries consisting of European (four cohorts:
640 ARIC, deCODE, Fenland, and UKB-PPP), African (two cohorts: ARIC and UKB-PPP), and East
641 Asian (one cohort: Kyoto University Nagahama East Asian cohort). All cohorts had proteomics
642 measured on the aptamer-based SomaScan assay v4 except for the UKB-PPP study, which used
643 the antibody-based Olink Explore 3072 platform.

644 **1.1. European ancestry cohorts**

646 We analyzed the GWAS of protein levels in individuals of European ancestry using four different
647 studies. Three of these four studies (ARIC, deCODE, and Fenland described below) had
648 proteomics measurements from the aptamer-based SomaScan assay v4 from SomaLogic
649 (Boulder, Colorado, USA). In brief, SomaScan assay v4 uses aptamers, which are single-
650 stranded oligonucleotides that have specific binding affinities to protein targets and can measure
651 up to 5,000 unique proteins. The UKB-PPP study had proteomics measurements from the
652 antibody-based Olink Explore 3072 platform, which measures up to 3,000 proteins. Briefly, Olink
653 (Uppsala, Sweden) uses proximity extension assay (PEA) technology, which detects proteins
654 through the binding of two separate antibodies carrying complementary oligonucleotide tags,
655 which hybridize to the protein target. We restricted our analyses to proteins encoded by autosomal
656 genes and analyzed a list of 4,687 proteins from SomaLogic and 2,823 proteins from Olink.

657 **1.1.1. ARIC**

659 The Atherosclerosis Risk in Communities (ARIC)¹³ measured protein levels from 9,084 American
660 participants of European and African ancestries using the SomaScan assay v4. Of these
661 participants, 4,657 plasma proteins were measured for 7,213 European American individuals.

662 **1.1.2. deCODE**

664 The deCODE study¹² provided 4,907 aptamers that measure 4,719 proteins in 35,559 Icelandic
665 individuals of European ancestry using SomaScan assay v4.

666 **1.1.3. Fenland**

668 The Fenland study¹¹ measured 4,775 proteins in 10,708 individuals of European ancestry using
669 SomaScan assay v4.

670 **1.1.4. UKB-PPP**

672 The UK Biobank Pharma Proteomics Project (UKB-PPP)¹⁴ conducted proteomic profiling on
673 54,219 individuals of multiple genetic ancestries in the UK Biobank using the Olink Explore 3072
674 platform. From this cohort, 34,557 European individuals, each with 2,923 unique proteins
675 measured, were utilized in the UKB-PPP as the discovery cohort, and we used this discovery
676 cohort in our study.

677 **1.2. African ancestry cohorts**

679 For African ancestries, we used GWAS of protein levels from two different studies (ARIC and
680 UKB-PPP) measured on SomaScan assay v4 and Olink Explore 3072, respectively.

681 **1.2.1. ARIC**

683 The ARIC cohort was previously described in the European cohort section and consists of 9,084
684 European American and African American individuals. Of these participants, 4,657 proteins from
685 the SomaScan v4 assay were measured for 1,871 African American individuals.

686 **1.2.2. UKB-PPP**

688 We used the African ancestry individuals from the UKB-PPP study, which consists of 931
689 individuals with 2,923 unique proteins measured with the Olink Explore 3072 platform.

690 1.3. East Asian ancestry cohort

692 Kyoto University Nagahama cohort

693 The Nagahama Primary Prevention Cohort Project (Kyoto-Nagahama cohort) is a joint project
694 between the Kyoto University Graduate School of Medicine and Nagahama City, Shiga Prefecture
695 that involved 10,000 residents of Nagahama ([https://w3.genome.med.kyoto-
696 u.ac.jp/en/nagahama-project/](https://w3.genome.med.kyoto-u.ac.jp/en/nagahama-project/)). Data generation was performed at the Kyoto University Center for
697 Genome Medicine, where 1,823 Japanese individuals of East Asian ancestry were whole
698 genome-sequenced and had 4,196 proteins measured using the SomaScan assay v4. Further
699 details can be found in **Supplementary Note 9**.

701 2. Identification of strict variant-to-gene (v2g) *cis*-protein quantitative trait loci (pQTLs)

702 Each cohort had had different *cis*-pQTL definitions. For example, the ARIC¹³ study defined *cis*-
703 pQTL as those within ± 500 kb of the TSS of the protein-coding gene with $FDR < 5\%$. The
704 deCODE study¹² defined *cis*-pQTL as those within ± 1 Mb of the TSS of the protein-coding gene
705 with $P < 1.8 \times 10^{-9}$. The Fenland Study¹¹ defined *cis*-pQTL as those within ± 500 kb of the
706 protein-coding gene with $P < 1.004 \times 10^{-11}$. The UKB-PPP¹⁴ noted that of their identified pQTLs,
707 66.9% of proteins tested (1,954 of 2,922 proteins) had a *cis*-pQTL within ± 1 Mb of the protein-
708 coding gene with $P < 1.7 \times 10^{-11}$. Thus, we created a common *cis* definition as follows.

709 2.1. Linkage disequilibrium (LD) clumping

710 We performed LD clumping (clumping window of 1 Mb, significance level of 5×10^{-8} , and clumping
711 r^2 threshold of 0.001) on each proteomic GWAS in each ancestry cohort. For European proteomic
712 GWAS, we used a reference panel composed of 50,000 randomly sampled unrelated UK
713 Biobank⁷⁰ individuals of European ancestry (UKB 50k). For African proteomic GWAS, we curated
714 an LD reference panel from the Human Genome Diversity Project and 1000 Genomes Project
715 (HGDP + 1kGP) reference panel⁷¹ for 994 African ancestry individuals. In East Asian ancestries,
716 we used the 1000 Genomes East Asian (1kGP EAS) reference panel. We retained variants with
717 a MAF > 0.01 in all reference panels.

720 2.2. Identification of *cis*- and *trans*-pQTLs

721 To determine *cis*-pQTLs, we used the Ensembl BioMart⁷³ package version Ensembl 105: Dec
722 2021 (Genome Reference Consortium Human Build 38, GRCh38.p13) to generate a human
723 protein-coding genes file. We considered relevant attributes such as the canonical TSS, gene
724 start, and gene end. Since Fenland proteomic GWAS were in GRCh37 coordinates, we
725 separately curated a protein-coding genes file using BioMart on the GRCh37 assembly in
726 Ensembl using version 110. For analysis, we excluded protein-coding genes located on sex
727 chromosomes and those located within the major histocompatibility complex (MHC) (GRCh38:
728 chr6 28,510,020– 33,480,577) due to the complex LD structure, high allelic diversity, and strong
729 pleiotropy in this region⁷⁴. We defined a *cis*-pQTL as a pQTL within ± 500 kb of the TSS of the
730 protein-coding gene. All other pQTLs were *trans*. We used *cis*-pQTLs since they are more likely
731 to directly impact the transcription and translation of the protein of interest.

732 2.3. Strict variant-to-gene *cis*-pQTL definition

733 To minimize potential horizontal pleiotropic effects, we defined a unique strict V2G definition for
734 *cis*-pQTLs whereby a *cis*-pQTL is a *strict V2G cis*-pQTL if it is a *cis*-pQTL for only one protein-
735 coding gene (*strict*) and it has the strongest link to the corresponding protein-coding gene based
736 on multiple sources of evidence and concomitantly has the highest Open Targets Genetics V2G
737 score (**Extended Data Fig. 1**). We outline these steps in the following two sections.

739
740
741
742
743
744
745
746
747
748
749
750
751
752
753
754
755
756
757
758
759
760
761
762
763
764
765
766
767
768
769
770
771
772
773
774
775
776
777
778
779
780
781
782
783
784
785
786
787
788
789

2.3.1. Strict *cis*-pQTL

For genome-wide significant independent *cis*-pQTLs in each cohort, we retained those associated with a single protein-coding gene. We defined this as a “strict” *cis*-pQTL definition. Here, we used *protein-coding genes* instead of *proteins (aptamers)* for the strict *cis* definition due to SomaScan assay v4 having multiple instances where two or more aptamers target a single protein, which would result in the unwarranted scenario where pQTLs that were *cis* for more than one aptamer of the same protein were removed.

2.3.2. Open Targets Genetics Variant-to-Gene (V2G)

We used the Open Targets Genetics³⁵ database (<https://genetics.opentargets.org/>) to determine whether each strict *cis*-pQTL held the highest V2G score for its corresponding associated protein-coding gene. This ensures that the variant is a suitable proxy for the plasma levels of the protein-coding gene. For instance, the variant may directly impact the protein-coding gene, potentially by altering its transcription, thereby influencing its plasma abundance. Briefly, Open Targets Genetics V2G scores are generated through a model trained on molecular QTLs (eQTL, sQTL, pQTL), chromatin interaction experiments such as promoter capture Hi-C (PCHi-C), *in silico* functional predictions such as Ensembl Variant Effect Predictor (VEP), and the distance between variants and genes' canonical transcription start sites. This composition of evidence enables accurate assignment of variants to genes. We note that the pQTL datasets utilized by Open Targets Genetics for model training are from earlier studies and do not overlap with the proteomics cohorts we analyzed in this study, mitigating the risk of overfitting.

Together, we combined the strict *cis* definition and V2G score from Open Targets Genetics to curate strict V2G *cis*-pQTLs, which decreases the chance of horizontal pleiotropy in MR.

3. Protein altering variant (PAV) and expression quantitative trait loci (eQTL)

Since pQTLs altering the binding epitope of a protein may reflect assay specificity instead of the true biological function of the protein^{1,64,75}, we annotated strict V2G *cis*-pQTLs as protein-altering variants (PAVs) of moderate or high impact if they or any variants in high LD ($r^2 > 0.8$) were identified as PAVs using VEP⁷⁶ (**Supplementary Tables 2–8**). VEP annotates the impact of variants into four categories: Modifier, Low, Moderate, or High (https://useast.ensembl.org/info/genome/variation/prediction/predicted_data.html). “Modifier” impact refers to variants in non-coding regions or affecting non-coding genes in which evidence of impact is hard to predict or limited. “Low” impact refers to variants that may not change protein behavior. “Moderate” impact variants are non-disruptive and may change protein effectiveness and include missense variants. “High” impact variants are disruptive and can cause truncation of proteins, loss of function, or trigger nonsense-mediated decay. If a strict V2G *cis*-pQTL and all of its LD proxies were labelled as Modifier or Low impact, we considered this strict V2G *cis*-pQTL to have no PAV. If a strict V2G *cis*-pQTL or any of its LD proxies were labeled Moderate or High, we considered this strict V2G *cis*-pQTL to be a PAV of -Moderate or -High impact, respectively.

We also conducted a *cis*-eQTL enrichment analysis using 49 tissues from GTEx v8 in European ancestries since if a *cis*-pQTL overlaps with the *cis*-eQTL of the same gene, it strengthens the evidence that the *cis*-pQTL acts directly on the gene products, reducing the risk of horizontal pleiotropy. To do so, we determined whether the strict V2G *cis*-pQTL was a *cis*-eQTL for the protein-coding gene of interest with $P < 1 \times 10^{-5}$ by querying 49 tissues in GTEx v8 European eQTLs. Querying was performed based on CHR:POS:EA:NEA and CHR:POS:NEA:EA (CHR: chromosome; POS: position; EA: effect allele; NEA: non-effect or other allele). In order to compare effect sizes across different cohorts, we aligned the strict V2G *cis*-pQTL effect allele in each cohort to the corresponding ancestry-specific reference panel's alternative allele (UKB 50k

790 for European, HGDP + 1kGP for African, and 1kGP EAS for East Asian ancestries). We note that
791 pQTLs in the Fenland cohort were based on GRCh37 coordinates and were lifted to GRCh38
792 prior to querying for *cis*-eQTLs across GTEx v8 tissues. After synchronizing the genome assembly,
793 7 out of 3,045 strict V2G *cis*-pQTLs in Fenland were automatically labeled as having no eQTL
794 since no corresponding GRCh38 coordinate existed for these variants, and 3,038 *cis*-pQTLs were
795 analyzed.

796 797 **4. GWAS outcome curation and selection**

798 We manually curated the latest and largest GWAS (as of February 2024) for European and African
799 ancestry outcomes. East Asian ancestry outcomes were selected from BioBank Japan¹⁵. All
800 GWAS in GRCh37 were lifted to GRCh38 with the liftOver tool. We outline the curation steps for
801 each ancestry's GWAS outcomes in detail:

802 803 **4.1. European ancestry outcomes**

804 During the curation, we considered 510 outcomes downloaded from 50 studies and one database.
805 We removed outcomes that were duplicated and had a larger GWAS available, had ambiguous
806 or broad definitions, were likely heterogeneous, were sex-specific, had missing relevant columns,
807 had no download link available, and were not relevant to our outcomes of interest. We retained
808 179 outcomes for analysis (**Supplementary Table 10**). We labeled rsids, chromosome, and
809 position if they were missing. Cases and sample sizes for each outcome were manually extracted
810 from the original manuscript or the supplementary tables of each corresponding study, and we
811 further categorized each outcome into one of 23 "Type" categories pertaining to the human
812 system the outcome was based on or most likely to fall under.

813 814 **4.2. African ancestry outcomes**

815 We manually curated 26 of the most up-to-date and publicly available African ancestry GWAS
816 summary statistics (**Supplementary Table 11**). Restricted access GWAS from dbGap were not
817 considered due to data access difficulties. Missing sample sizes were manually annotated with
818 the sample size by inspecting the original manuscript and Supplementary Tables, while missing
819 rsids were labeled using the HGDP + 1kGP reference panel. We annotated missing chromosomes
820 and positions and used VEP to annotate variants missing effect allele frequency with
821 gnomADg_AFR_AF (gnomAD genomes for African/American populations). We categorized each
822 outcome into one of 8 "Type" categories, including Respiratory, Musculoskeletal, Cardiovascular,
823 Eye, Anthropometry, Biomarker, Psychiatric, and Metabolic/endocrine.

824
825 As exploratory analyses, we included 114 binary cardiovascular and 9 binary autoimmune-related
826 outcomes from the Million Veteran Program ($n = 635,969$) for African individuals.

827 828 **4.3. East Asian ancestry outcomes**

829 We curated 220 outcomes from Biobank Japan (<https://pheweb.jp/>)²⁷. We excluded 14 sex-
830 specific outcomes, including Abortion, Breast cancer, Cervical cancer, Cesarean section, Ectopic
831 pregnancy, Endometriosis, Endometrial cancer, Mastopathy, Ovarian cancer, Ovarian cyst, Pre-
832 eclampsia, Prostate cancer, Uterine fibroid, and Uterine prolapse. We analyzed 206 outcomes
833 (**Supplementary Table 12**). We also provide "Type" labels for each outcome, denoting the human
834 system the outcome was based on or was most likely related to.

835 836 **5. Two-sample Mendelian randomization**

837 To assess the putative causal effect of protein abundance on outcomes in European, African, and
838 East Asian ancestries, we performed two-sample MR using TwoSampleMR v.0.5.7⁷⁷. To mitigate
839 horizontal pleiotropy, we used strict V2G *cis*-pQTLs as instrumental variables to proxy protein-
840 level exposures, as defined in the earlier sections of the methods. We harmonized exposure and

841 outcome GWAS using the `harmonise_data()` function and performed a proxy search if an
842 instrument was absent in the outcome GWAS. For European, African, and East Asian ancestries,
843 we used the UKB 50k, HGDP + 1kGP, and 1kGP East Asian reference panels that were
844 previously used for LD clumping for the proxy search, respectively. We searched for proxies using
845 PLINK v.1.9⁷² parameters `--ld-window=5000`, `--ld-window-kb=5000`, `--ld-window-r2=0.8` and
846 retained proxies with minor allele frequencies ≤ 0.42 .

847
848 MR analyses were performed using the `mr()` function. For proteins with a single genetic instrument,
849 the association between the protein and outcome was evaluated using a Wald ratio estimate. For
850 proteins with ≥ 2 genetic instruments, we used an inverse variance weighted random effects
851 estimate. We determined whether genetic instrumental variables had F-statistics $> 10^{43,78}$,
852 indicating strong associations with the exposure and thus less chance of weak instrument bias,
853 which may bias the causal effect estimates towards the null in two-sample MR. F-statistics are
854 shown in **Supplementary Table 9**. We corrected for multiple testing per cohort in each ancestry
855 by applying a Benjamini-Hochberg-corrected P threshold (FDR)⁴⁵ of 0.05 (5%) as done
856 previously¹⁹.

857
858 We note that beta estimates from MR for continuous traits are not directly comparable across
859 different outcomes because the units used in GWAS vary. For instance, some GWAS use clinical
860 units, whereas others use standardized and/or residualized values.

861 862 **6. MR sensitivity analyses**

863 To increase the robustness of MR findings, we further filtered MR results based on multiple
864 sensitivity analyses, including heterogeneity tests, MR using alternative approaches (including
865 weighted median, weighted mode, MR-Egger), and Steiger directionality test⁷⁹ to assess reverse
866 causality. Following these filtering steps, we refer to retained protein-phenotype associations as
867 “MR-passing”. The sensitivity analyses are described for proteins with ≥ 2 instruments and
868 proteins with ≥ 3 instruments below:

869 870 **6.1. Sensitivity analyses for proteins with two or more instruments**

871 The heterogeneity test was performed for proteins with ≥ 2 instruments and describes whether
872 strict V2G *cis*-pQTLs of the same protein are likely to show comparable effects on the tested
873 outcomes. For heterogeneity testing, we used the `mr_heterogeneity()` function to compute a
874 heterogeneity P value (`Q_pval`), and we calculated I^2 statistics using the `lsq()` function. If an
875 association had an I^2 threshold ≥ 0.5 and a heterogeneity P value (`Q_pval`) < 0.05 , this indicated
876 considerable heterogeneity.

877 878 **6.2. Sensitivity analyses for proteins with three or more instruments**

879 For proteins with ≥ 3 genetic instruments, we performed additional sensitivity analyses with
880 alternative MR methods such as MR weighted median, MR weighted mode, and MR-Egger
881 methods, as well as Steiger directionality testing. To check the consistency of MR estimates, we
882 required the MR estimate, as well as the sensitivity analyses estimates from the MR weighted
883 median, MR weighted mode, and MR-Egger approaches, to all have the same sign. For
884 directional pleiotropy, we used the `mr_pleiotropy_test()` function to perform the MR-Egger
885 intercept test and considered a P value < 0.05 as a statistically significant deviation from the null
886 and an indication of directional pleiotropy. We also performed Steiger filtering on all proteins
887 (`directionality_test()` function). Any pQTLs that explain more variance in the outcome than in the
888 exposure potentially indicate reverse causation and were removed from further analysis.

889 890 **7. Colocalization of proteomic GWAS with outcome GWAS**

891 To assess whether plasma protein levels share the same causal variant with GWAS outcomes,
892 we employed two colocalization methods to ensure the robustness of our findings. We performed
893 PWCoCo^{18,36} and SharePro⁸⁰ for MR associations that passed all MR sensitivity analyses
894 described in the previous section. PWCoCo and SharePro are recent methods allowing multiple
895 independent associations to be assessed. Both improve on the original coloc method⁸¹, which
896 was limited by the assumption that a single variant exists per GWAS, wherein the method only
897 considers the strongest of these distinct association signals when multiple independent
898 associations exist. A detailed description of both methods is provided in **Supplementary Note**
899 **10**. Colocalization analyses were performed around a 1-Mb region centered on the lead (lowest
900 *P* value) *cis*-pQTL. We set a colocalization posterior probability (PP) of a shared causal variant \geq
901 0.8 in any of PWCoCo or SharePro as evidence of colocalization. For simplicity, we report the
902 maximum PP between PWCoCo and SharePro (PP_{max}) in the main text. We reported putatively
903 causal associations (**Supplementary Tables 14–16**) as associations which pass all MR
904 sensitivity analyses, Steiger filtering, and also colocalized with a PP \geq 0.8 in any one of PWCoCo
905 or SharePro. Due to the difficulty in verifying the corresponding Olink assay target for each
906 SomaScan aptamer, we counted unique protein-phenotype associations using protein-coding
907 genes to harmonize between proteomics platforms. **Supplementary Tables 14–16** contain MR
908 and colocalization summaries, summaries of effect direction consistency across cohorts, flags of
909 proteins instrumented by PAVs of high impact, and whether the protein-phenotype association
910 came from a protein uniquely instrumentable in that ancestry. We also annotate whether protein-
911 phenotype associations passed the most stringent Bonferroni correction for the total number of
912 MR tests across three ancestries ($P < 0.05 / 874,465$).

913 8. Distinguishing between previously reported and unreported protein-phenotype pairs

914 8.1. Comparing against earlier studies identifying putatively causal protein-phenotype pairs with

915 MR and colocalization evidence

916 MR and colocalization evidence

917 To identify the status of protein-phenotype associations as reported or unreported (not found from
918 pre-existing proteome-phenome-wide MR studies) in European ancestries, we overlapped our
919 associations with recent proteome-phenome-wide MR analyses from Zheng et al. 2020¹⁸ and
920 multi-ancestry proteome-wide MR analyses from Zhao et al. 2022¹⁹. We used the 111 identified
921 putatively causal associations (65 proteins on 52 phenotypes) from “Table S7” of Zheng et al.¹⁸
922 and the 45 associations from “ST7A” of Zhao et al.¹⁹.

923 We note that Zhao et al. used three colocalization methods and a more relaxed threshold of PP
924 > 0.7 as evidence of colocalization. To do so, we harmonized the outcomes from Zheng and Zhao
925 to our outcomes and matched protein-phenotype pairs using ensembl ID and outcome name for
926 the Zheng study and UniProt ID and outcome name for the Zhao study. Any of our identified
927 putatively causal European ancestry association pairs not from these two studies were identified
928 as unreported.

929 For African ancestries, we overlapped our protein-phenotype pairs with the single protein-
930 phenotype pair passing FDR correction identified in “ST8A” of Zhao et al.¹⁹. Any pairs that did not
931 overlap were considered unreported.

932 9. Protein-phenotype network plots

933 We used Python igraph (v.0.10.8) to generate networks. Placement of nodes was generated
934 in Cytoscape (v.3.10.2) and manual editing was performed in Adobe Illustrator (v.28.2).

935 10. Effect concordance within-ancestry

936 To determine the concordance of MR effect estimates within European and African ancestries,
937 which both included more than one proteomics cohort, we compared protein-coding genes to
938

942 harmonize assay names across SomaScan assay v4 and Olink 3072 Explore platforms. However,
943 we could not verify whether Olink assays for a particular protein targeted the same domain as its
944 corresponding SomaScan assay, which may lead to differences in MR estimates. Moreover, since
945 some proteins were instrumented by *cis*-pQTLs that may be PAVs of high impact, which could
946 also lead to discordance in effects, we annotated these associations with a flag and advise caution
947 in the interpretation of these flagged results (**Supplementary Tables 14–16**).

948
949 **11. Druggability assessment**
950 We performed a druggability assessment on instrumentable protein-coding genes and protein-
951 phenotype associations that showed putatively causal relationships.

952 953 **11.1. Druggability assessment of instrumentable proteins**

954 For instrumentable protein-coding genes, we determined druggability based on Finan et al.³⁸, as
955 described below.

956 957 **11.1.1. Finan et al.**

958 Finan et al.³⁸ considered 20,300 protein-coding genes annotated using Ensembl version 73 and
959 classified 4,479 (22%) into three tiers (Tier 1, 2, and 3) as drugged or druggable. Tier 1 (1,427
960 genes) encompasses the primary targets of approved small molecules and biotherapeutic drugs,
961 along with those influenced by clinical-phase drug candidates. Tier 2 (682 gene) involves proteins
962 closely associated with drug targets or linked to drug-like compounds. Meanwhile, Tier 3 (2,370
963 genes) comprises secreted or extracellular proteins that are distantly related to approved drug
964 targets, and those in important druggable gene families not covered in Tiers 1 or 2. We denoted
965 all other protein-coding genes that did not fall in Tier 1, 2, or 3 categories as “Unclassified”. To
966 check the overlap of protein-coding genes across all cohorts when stratifying into Finan et al. tiers
967 (**Supplementary Figure 5 and 6**), we used the UpSetR⁸² package v.1.4.0
968 (<https://github.com/hms-dbmi/UpSetR>).

969 970 **11.2. Druggability assessment and enrichment of protein-phenotype pairs**

971 We first assessed how many proteins from the identified pairs of putatively causal protein-
972 phenotype associations had existing drugs by querying DrugBank³⁹. We used Ensembl ID to
973 match protein targets in DrugBank. Next, we created heatmaps using the pheatmap package
974 v.1.0.12 in R incorporating the druggable genome, Drugbank, and Open Targets Platform
975 (described below). We overlapped protein-phenotype pairs with the DrugBank database to
976 determine whether any drugs existed for these disease-implicated proteins while Open Targets
977 was used to determine whether any clinical trial information existed for these proteins.

978 979 **11.2.1. DrugBank**

980 We used DrugBank database v.5.1.12 (<https://go.drugbank.com/releases/latest>) and R package
981 dbparser v.2.0.2 to parse the DrugBank database xml file. We aggregated drugs and target
982 information and overlapped this with putatively causal protein-phenotype associations to
983 determine which proteins had an available drug.

984 985 **11.2.2. Open Targets**

986 We used Open Targets v.24.03 (<https://platform.opentargets.org/downloads>). We used the
987 knownDrugsAggregated dataset, which provides information on known drugs for a given disease
988 and contains protein target information. Open Targets also includes information on clinical trials
989 and its phases, which we used to determine the status of a protein target and its corresponding
990 drug. We overlapped this dataset by matching Ensembl ID with our identified protein-phenotype
991 associations.

992

993 12. Follow-up analyses showing evidence for IL1RL1

994 We filtered protein-phenotype associations in European ancestries by ensuring that the protein
995 was instrumented in two or more ancestries, was targeted by both SomaScan and Olink assays,
996 had an MR effect that was concordant across all cohorts, had MR and colocalization evidence in
997 three or more cohorts for the protein-phenotype pair, and was implicated in at least one binary
998 phenotype. Following these filtering steps, we identified 53 candidate protein-phenotype pairs and
999 highlighted IL1RL1 in IBD, CD, and UC as an illustrative example.

1000

1001 *12.1. MR and colocalization of IL1RL1 in East Asian ancestry with IBD, CD, and UC*

1002 To validate that IL1RL1 was also putatively causal for IBD, CD, and UC in non-European
1003 ancestries, we performed two-sample MR and colocalization with PWCoCo and SharePro using
1004 the IL1RL1 strict V2G *cis*-pQTL (rs12712135) identified in the Kyoto University Nagahama East
1005 Asian ancestry proteomics cohort. We used the largest East Asian ancestry GWAS for IBD
1006 (14,393 cases and 15,456 controls), CD (7,372 cases and 15,456 controls), and UC (6,862 cases
1007 and 15,456 controls) from Liu et al.⁶⁵. Harmonization was performed similarly to the primary
1008 analyses, and we used the Wald ratio to obtain MR effect estimates. Colocalization was
1009 performed as described in earlier sections of the methods, and we used $PP \geq 0.8$ as the threshold
1010 for evidence of colocalization in any of PWCoCo or SharePro.

1011

1012 *12.2. MR of IL1RL1 in African ancestry with IBD and UC*

1013 We estimated the causal effect of IL1RL1 on IBD (1,285 cases and 119,314 controls) and UC
1014 (857 cases and 119,909 controls) in African ancestry using outcome GWAS from the Million
1015 Veteran Program⁵⁷. We performed MR using the IL1RL1 strict V2G *cis*-pQTL (rs1420101) in the
1016 ARIC and UKB-PPP African ancestry cohorts. The Wald ratio was used to obtain MR effect
1017 estimates.

1018

1019 *12.3. Cox regression analysis for 10-year cumulative events of IBD, CD, and UC in the UK Biobank*

1020
1021 We used multivariable Cox proportional hazards regression to determine whether baseline
1022 plasma IL1RL1 protein level was associated with cumulative events of IBD, CD, or UC. We
1023 adjusted for age, sex, recruitment center, Olink measurement batch, Olink processing time, and
1024 the first 10 genetic principal components (UKB field: 22009) to adjust for genetic ancestry while
1025 protein levels were rank-based inverse normal transformed. We used the `coxph()` function from
1026 the survival R package v.3.2.13 and considered $P < 0.05$ as nominal significance of association.
1027 None of the genetic principal components were significantly associated with the IBD, CD, and UC
1028 outcome in each analysis.

1029

1030 We checked the proportional hazards assumption using the `cox.zph()` function for the IL1RL1
1031 association analysis for IBD, CD, and UC for the rank-based inverse normal transformed IL1RL1
1032 covariate. The proportional hazards assumption tests the null hypothesis that each covariate's
1033 effect estimate does not vary with time. We used the "GLOBAL" variable from `cox.zph()` which
1034 tests the null hypothesis of whether all inputted covariates meet the proportional hazards
1035 assumption. We considered $P < 0.05$ as evidence that the proportional hazards assumption was
1036 not fulfilled.

1037

1038 We defined IBD using ICD10 codes K50-K51, CD using K50, and UC using K51. We calculated
1039 the time to event by subtracting the date of event registration from the date of enrollment (data
1040 field: 53), focusing on events occurring within 10 years of enrollment. We excluded cases of
1041 prevalent IBD that met these criteria before enrollment, and those without a recorded event date
1042 for IBD, and performed the same steps for CD and UC. Controls for the IBD analysis were defined
1043 as individuals without an IBD, UC, or CD record based on self-reported medical history. Controls

1044 for the CD analysis were defined as individuals without a CD record, and controls for the UC
1045 analysis were defined as individuals without a UC record, based on self-reported medical history.
1046 We analyzed 333 cases and 40,001 controls for IBD, 130 cases and 40,388 controls for CD, and
1047 240 cases and 40,178 controls for UC.

1048
1049 We plotted Kaplan-Meier curves by stratifying individuals into the bottom 25% and the top 25%
1050 based on baseline plasma *IL1RL1* levels. We performed a log-rank test to assess whether there
1051 is a statistically significant difference in survival between these two groups, with a nominal $P <$
1052 0.05.

1053
1054 **12.4. Bulk RNA-sequencing**
1055 We used the IBD Transcriptome and Metatranscriptome Meta-Analysis (IBD TaMMA) platform⁶⁷
1056 (<https://ibd-meta-analysis.herokuapp.com>) to evaluate changes in *IL1RL1* gene expression. IBD
1057 TaMMA encompasses 3,853 RNA-Seq datasets from 26 studies on IBD and control samples
1058 across various tissues. All datasets were processed using a uniform computational pipeline and
1059 underwent batch correction for harmonizing data, enabling consistent comparison across studies.
1060 Differential expression results for ileum, colon, and rectum biopsies from CD and UC patients
1061 versus healthy controls were downloaded from IBD TaMMA. We assessed the log₂ fold change
1062 to create forest plots.

1063
1064 **12.5. Single-cell RNA-sequencing**
1065 To gain a better understanding of the enrichment of *IL1RL1* in specific cell types, we obtained
1066 single-cell RNA sequencing data from Kong et al.⁶⁶ (SCP1884 from
1067 <https://singlecell.broadinstitute.org/>), which profiled 720,633 cells from the terminal ileum and
1068 colon of 71 CD individuals with different levels of inflammation. Specific details of sample
1069 collection, data processing, and single-cell profiling have been described previously⁶⁶. We
1070 evaluated the normalized gene expression levels of *IL1RL1* in 25 different cell types and replotted
1071 the first two dimensions of Uniform Manifold Approximation and Projection (UMAP) coordinates
1072 to visualize the cell clusters. To determine if *IL1RL1* was more significantly expressed in certain
1073 cell types, we conducted 5,000 permutations of the cell type labels. We assessed how often a
1074 specific cell type had the same or a higher proportion of cells expressing *IL1RL1* compared to all
1075 the cells in the overall population (permutation P value).

1076
1077 **13. STROBE-MR statement**
1078 Our study closely adheres to the STROBE-MR guidelines and the STROBE-MR checklist is
1079 attached in **Supplementary Note 11**.

1080
1081 **14. Ethics declarations**
1082 All contributing cohorts obtained ethical approval from their institutional ethics review boards. The
1083 contributing proteomics cohorts include the Atherosclerosis Risk in Communities (ARIC) Study,
1084 deCODE study, Fenland study, UK Biobank, and Kyoto University Nagahama study. The UK
1085 Biobank has approval from the North West Multi-centre Research Ethics Committee as a
1086 Research Tissue Bank.

1087
1088 **15. Data availability**
1089 We will provide unfiltered proteome-phenome wide MR results for European (ARIC, deCODE,
1090 Fenland, UKB-PPP), African (ARIC, UKB-PPP), and East Asian (Kyoto University Nagahama
1091 cohort) ancestries on FigShare upon publication. We caution against directly comparing MR effect
1092 estimates across continuous outcomes, as the outcomes were collected from various sources
1093 and may not be scaled to the same units.

1094

1095 [15.1. Proteomic GWAS](#)

1096 ARIC summary statistics (EUR and AFR): <http://nilanjanchatterjeelab.org/pwas/>
1097 deCODE summary summary statistics (EUR): <https://www.deCODE.com/summarydata/>
1098 Fenland summary statistics (EUR): <https://omicscience.org/apps/pgwas/>
1099 UKB-PPP summary statistics (EUR, AFR): <http://ukb-ppp.gwas.eu/>
1100 Kyoto University Nagahama cohort summary statistics (EAS): Available through contacting the
1101 authors of this study.

1102 [15.2. Outcome GWAS summary statistics](#)

1103 Information on the 179 European outcomes used in this study and the link to the original summary
1104 statistics is available in **Supplementary Table 10**.
1105 The 26 African outcomes are available in **Supplementary Table 11**.
1106 The 206 East Asian outcomes are available in **Supplementary Table 12**.
1107 Million Veteran Program outcomes can be found in the original study⁵⁷.
1108 The largest East Asian ancestry IBD, CD, and UC GWAS are publicly available from Liu et al.⁶⁵
1109 and were downloaded from <https://www.ibdgenetics.org/>
1110

1111 [15.3. Variant-to-gene score](#)

1112 Open Targets Genetics³⁵ (<https://genetics-docs.opentargets.org/data-access/data-download>),
1113

1114 [15.4. Reference panels](#)

1115 European ancestries: UKB 50k (<https://www.ukbiobank.ac.uk/>)
1116 East Asian ancestries: 1000 Genomes Project (<https://www.internationalgenome.org/data>)
1117 African ancestries: HGDP+1KG (<https://gnomad.broadinstitute.org/news/2020-10-gnomad-v3-1-new-content-methods-annotations-and-data-availability/#the-gnomad-hgdp-and-1000-genomes-callset>)
1118
1119

1120 [15.5. Druggability](#)

1121 We used Finan et al. 2017³⁸ for the list of 4,479 protein-coding genes in each druggability tier,
1122 DrugBank database v.5.1.12 (<https://go.drugbank.com/releases/latest>) for information on drugs
1123 targeting specific proteins, and Open Targets Platform database v.24.03
1124 (<https://platform.opentargets.org/downloads>) for clinical trial phase and status information for
1125 protein-drug-disease triplets.
1126
1127

1128 [15.6. Expression analyses](#)

1129 For gene expression data, we used data from Kong et al.⁶⁶ (SCP1884 at Single Cell Portal
1130 <https://singlecell.broadinstitute.org/>).
1131

1132 [16. Code availability](#)

1133 We used R v.4.1.2 (<https://www.r-project.org/>),
1134 Python 3.10 (<https://www.python.org/downloads/release/python-3100/>)
1135 PLINK v.1.9⁷² (<http://pngu.mgh.harvard.edu/purcell/plink/>),
1136 TwoSampleMR v.0.5.6 (<https://mrcieu.github.io/TwoSampleMR/>),
1137 coloc v.5.2.3⁸¹ (<https://chr1swallace.github.io/coloc/>),
1138 PWCoCo^{18,36} (<https://github.com/jwr-git/pwcoCo>),
1139 SharePro v.5.0.0⁸⁰ (https://github.com/zhwm/SharePro_coloc/),
1140 Cytoscape v.3.10.2 (<https://cytoscape.org/>),
1141 LocusZoom⁸³ (<https://my.locuszoom.org/>)
1142

1143 Code used in this study will be made available at <https://github.com/chenyangsu/pQTL-MR> upon
1144 publication.
1145

1146

1147 **17. Acknowledgments**

1148 This research has been conducted using the UK Biobank Resource under Application Number
1149 27449. C.-Y.S. is supported by a CIHR Canada Graduate Scholarship Doctoral Award (Funding
1150 Reference Number: 187673), an FRQS doctoral training scholarship, and a Lady Davis
1151 Institute/TD-Bank Scholarship. T.L. has been supported by start-up funding from the Office of the
1152 Vice Chancellor for Research and Graduate Education, School of Medicine and Public Health,
1153 and Department of Population Health Sciences at the University of Wisconsin-Madison. S.Y. is
1154 supported by the Japan Society for the Promotion of Science.

1155

1156 The funders had no role in the study design, data collection and analysis, decision to publish, or
1157 preparation of the manuscript. We acknowledge Servier Medical Art (<https://smart.servier.com/>)
1158 for providing images that were used to create diagrams in this study.

1159

1160 **18. Author contributions**

1161 Conception and design: C.-Y.S., T.L., S.Y.

1162 Methodology: C.-Y.S., W. Z., T.L., S.Y.

1163 Data curation: C.-Y.S., S.S.-H., T.-Y.Y., K.Y.H.L., Y.C., F. M., T.L., S.Y.

1164 Data Analysis: C.-Y.S., T.L., S.Y.

1165 Visualization: C.-Y.S., A.v.d.G., T.L., S.Y.

1166 Knowledge portal: C.-Y.S., D.-K.J., M.C., S.Y.

1167 Writing—Original Draft: C.-Y.S.

1168 Writing—Review and Editing: all authors

1169 Supervision: T.L., S.Y.

1170 Project administration: T.L., S.Y.

1171 Funding acquisition: V.M., S.Z., T.L., S.Y.

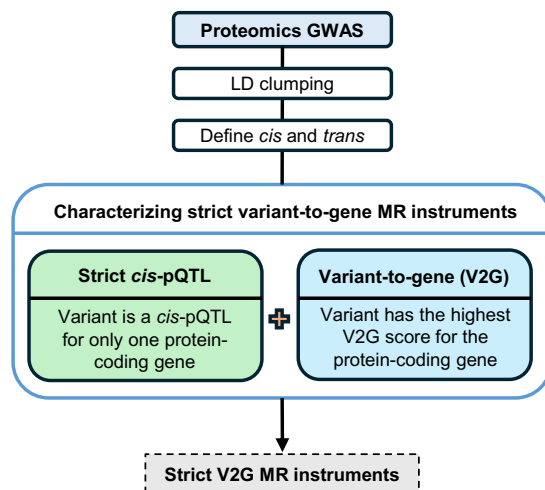
1172

1173 **19. Competing Interests**

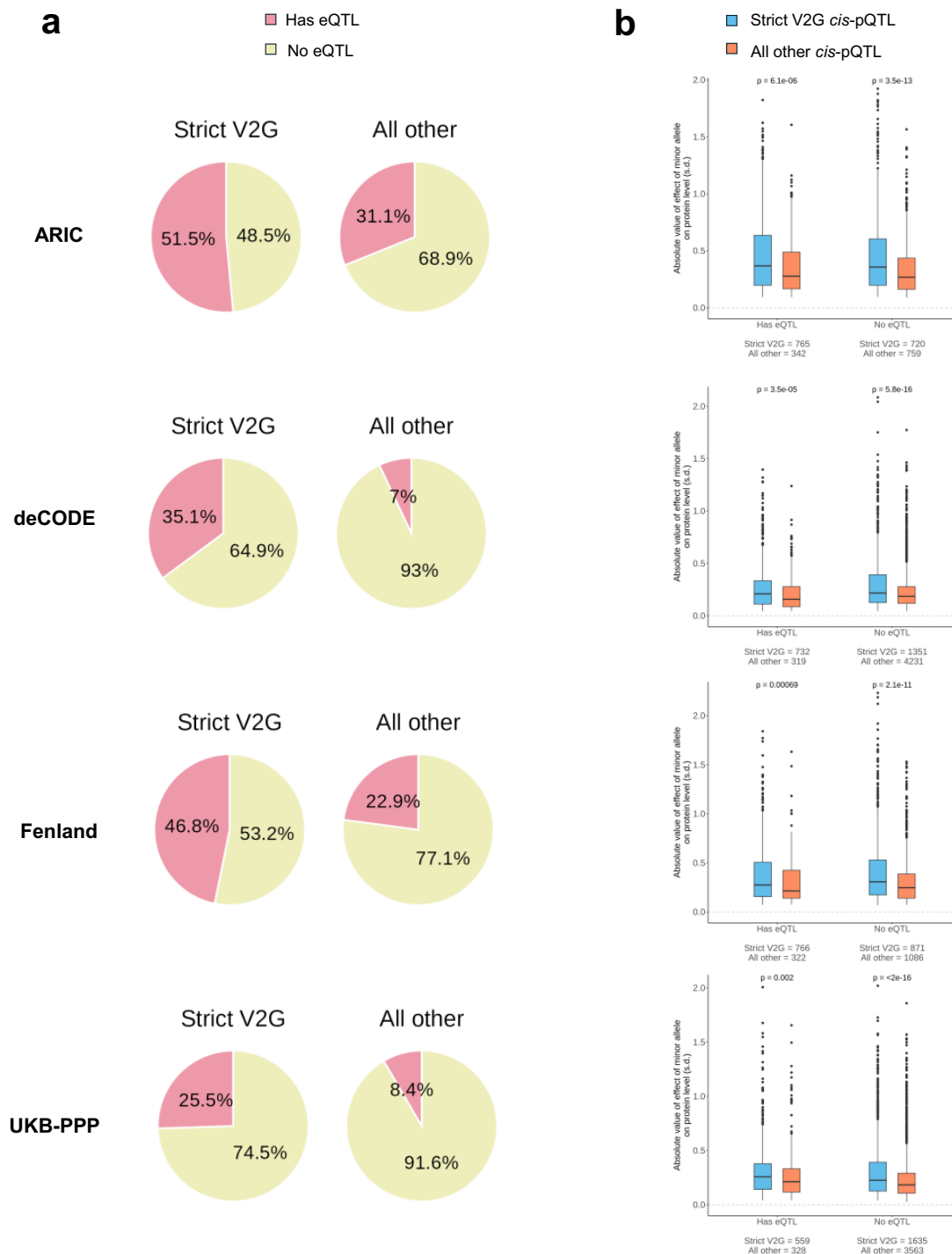
1174 Y.C. is an employee, J.B.R. is the CEO, and W.Z., G.B.-L., and T.L. have been consulting for 5
1175 Prime Sciences. However, this study was performed separately with no relationship to 5 Prime
1176 Sciences. J.B.R.'s institution has received investigator-initiated grant funding from Eli Lilly,
1177 GlaxoSmithKline and Biogen for projects unrelated to this research. The other authors declare no
1178 conflict of interest.

1179

1180 **Extended Data Figures**
1181



1182
1183 **Extended Data Fig. 1. Flow diagram showing the definition of strict variant-to-gene**
1184 **cis-pQTLs.**
1185 Flow diagram showing the selection of strict variant-to-gene (V2G) cis-pQTLs used as instruments
1186 for MR starting from the proteomic GWAS.

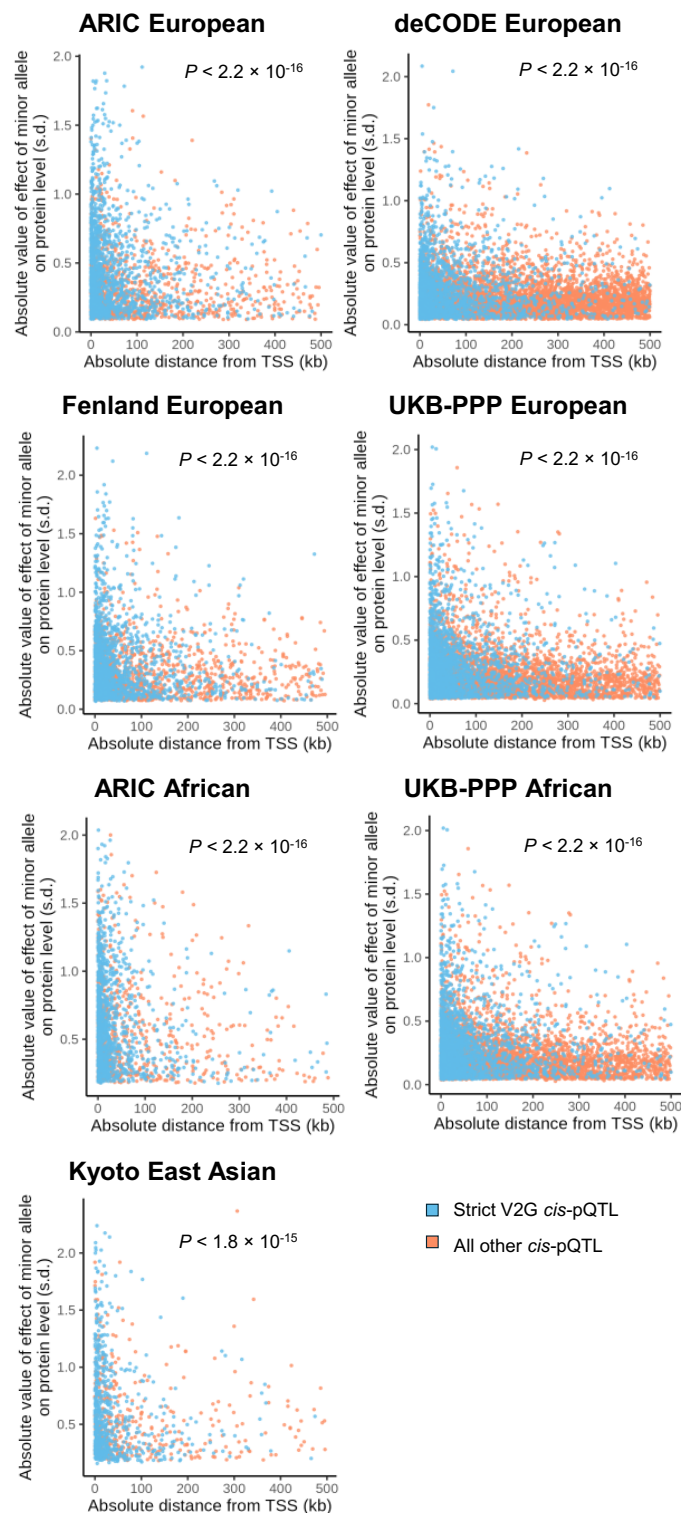


1187
1188
1189
1190
1191
1192
1193
1194
1195

Extended Data Fig. 2. eQTL enrichment analysis comparing strict V2G *cis*-pQTLs against all other *cis*-pQTLs.

- (a) Pie charts showing proportion of eQTL enrichment in the ARIC, deCODE, Fenland, and UKB-PPP European ancestry cohorts for strict V2G *cis*-pQTLs compared to all other *cis*-pQTLs. Red: presence of a *cis*-eQTL; Yellow: absence of a *cis*-eQTL.
- (b) Absolute value of effect of the minor allele on protein level broken down by the presence or absence of *cis*-eQTLs in the ARIC, deCODE, Fenland, and UKB-PPP European

1196 ancestry cohorts. Strict V2G, strict variant-to-gene *cis*-pQTLs; All other, all other *cis*-
1197 pQTLs that were removed due to strict V2G filtering. Boxplots show the median, lower,
1198 and upper quartiles; whiskers end at 1.5 times the interquartile range from the top and
1199 bottom of the box; points outside the whisker boundaries are plotted individually; smaller
1200 black dots represent individual points and are used to show the number of samples
1201 included in each boxplot; significance level *P* value is based on the Mann-Whitney U test.
1202

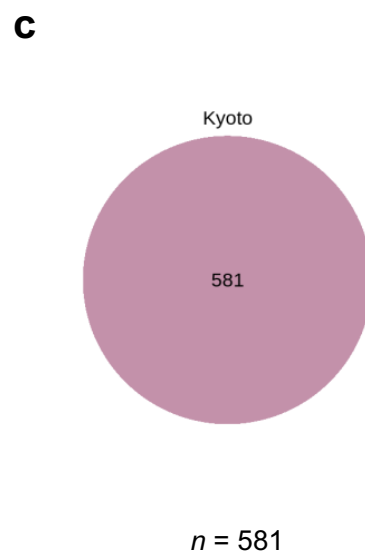
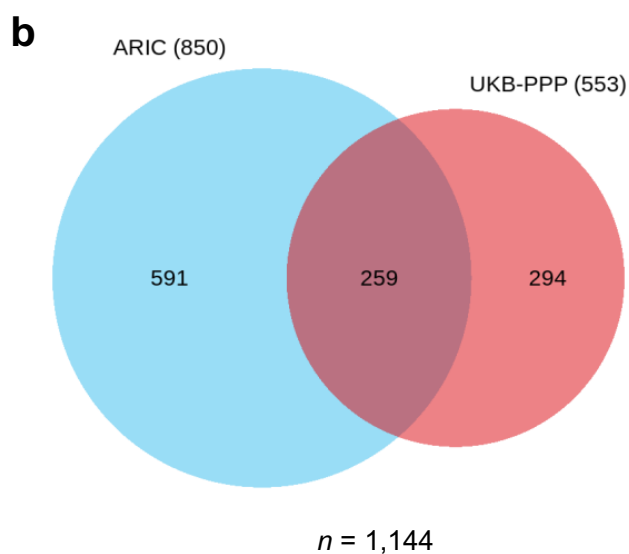
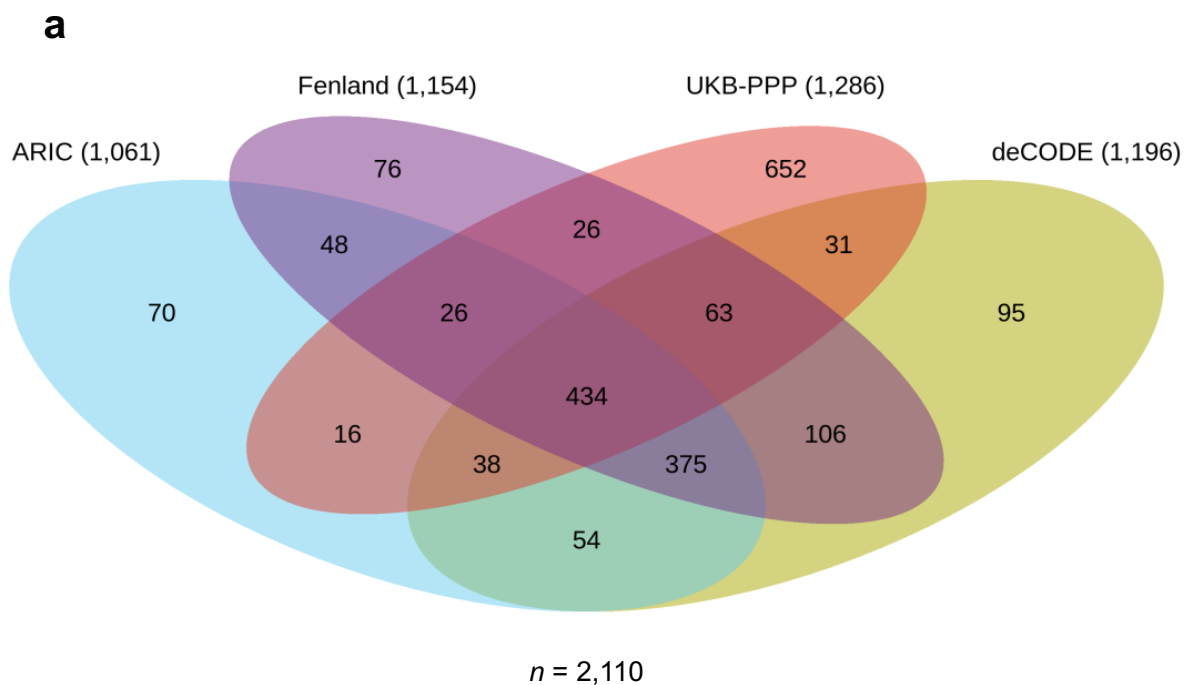


1203 **Extended Data Fig. 3. Absolute distance from transcription start site versus effect size for**
1204 **strict V2G *cis*-pQTLs and all other *cis*-pQTLs.**
1205

1206 The x-axis shows the distance of the pQTL from the canonical transcription start site of the
1207 associated protein-coding gene while the y-axis shows the absolute value of the effect size
1208 estimate of the effect allele aligned to the minor allele of each ancestry's respective reference
1209 panel. (Note, in European, African, and East Asian ancestry proteomics cohorts, the effect allele

1210 of *cis*-pQTLs in each cohort was aligned to the minor allele of the corresponding variant in their
1211 respective reference panels—UKB 50k for European, HGDP+1kGP for African, and 1kGP for
1212 East Asian ancestry—to harmonize alleles across each ancestral cohort for plotting). Strict V2G
1213 *cis*-pQTLs are highlighted in blue while all other *cis*-pQTLs are highlighted in orange. Note that
1214 Fenland European *cis*-pQTLs are presented in GRCh37 coordinates while all other cohorts are
1215 presented in GRCh38 coordinates. *P* values show a one-sided t-test testing whether strict V2G
1216 *cis*-pQTLs have smaller absolute distance to the TSS compared to all other *cis*-pQTLs.
1217
1218

1219



Extended Data Fig. 4. Within ancestry comparison of instrumentable proteins.

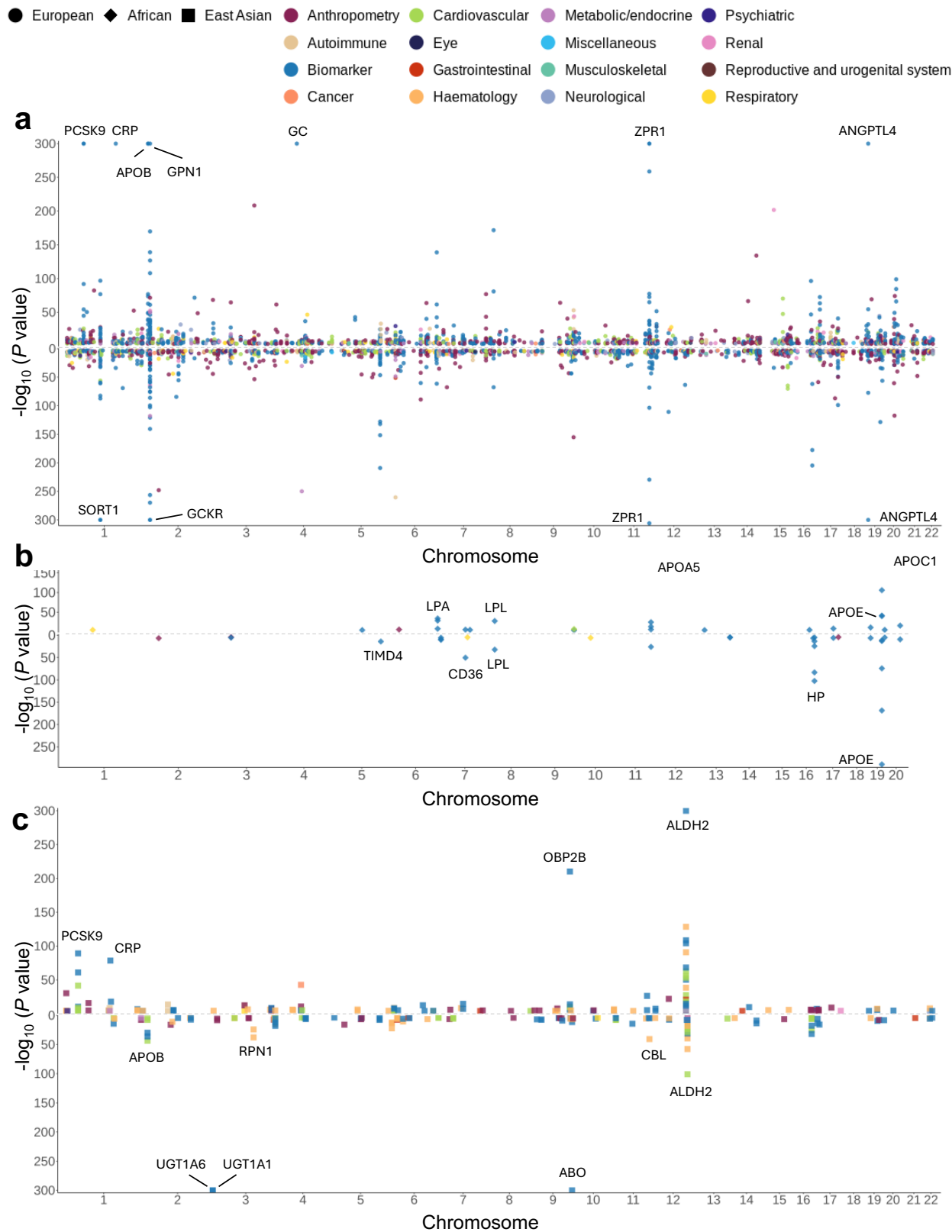
Venn diagrams of overlapping instrumentable proteins within ancestries.

(a) European cohorts involving ARIC, deCODE, Fenland, and UKB-PPP (4 cohorts).

(b) African cohorts involving ARIC and UKB-PPP (2 cohorts).

(c) East Asian ancestry cohort from Kyoto University Nagahama (single cohort).

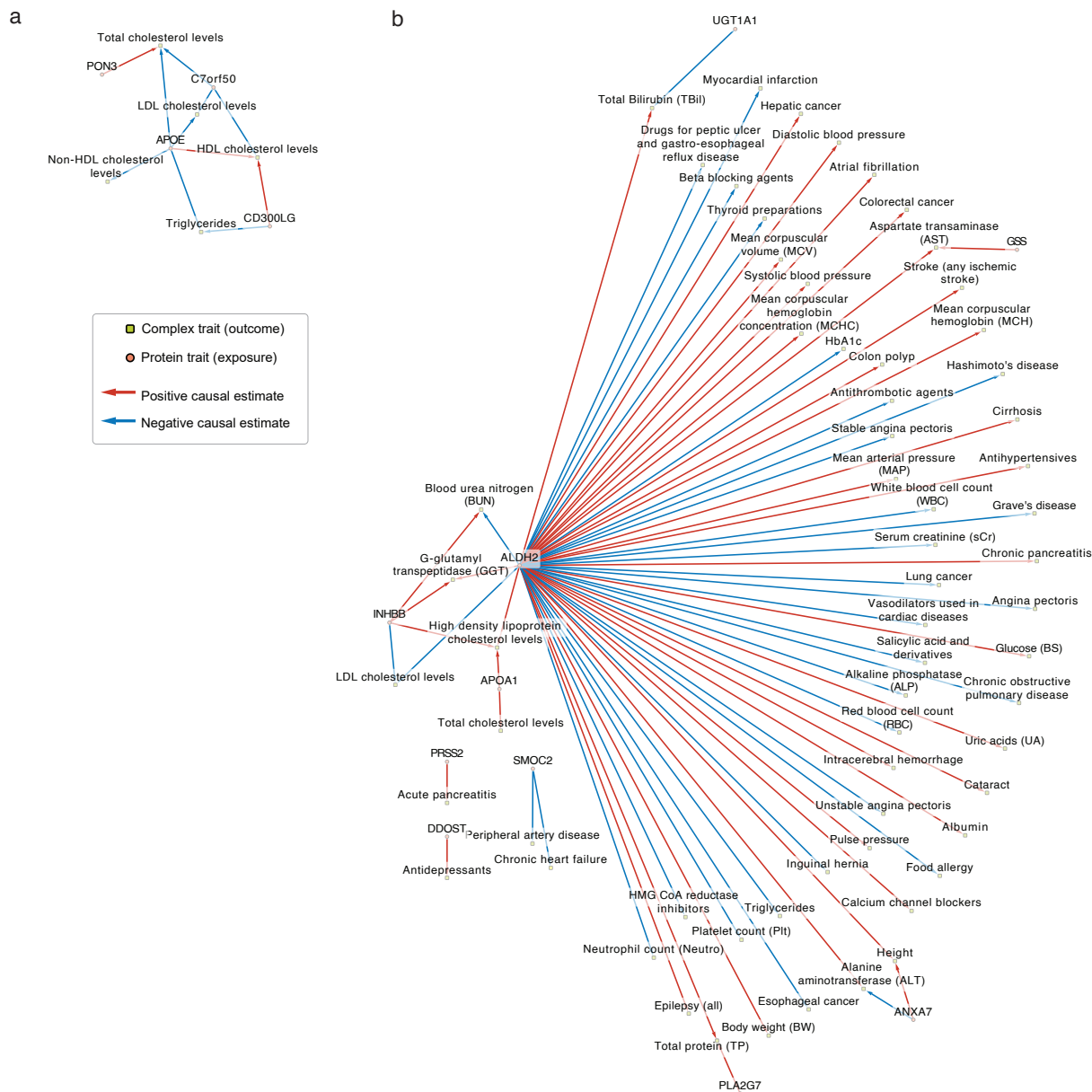
1220
1221
1222
1223
1224
1225
1226



1227
1228
1229

Extended Data Fig. 5. Putatively causal protein-phenotype associations across European, African, and East Asian ancestries.

1230 Miami plots displaying chromosomal position (*x*-axis) of significant putatively causal protein-
1231 outcome associations (MR-passing and colocalized with $PP_{\max} \geq 0.8$) in (a) European, (b) African,
1232 (c) East Asian ancestry. The *y*-axis shows *P* values from the MR causal estimates where the
1233 exposure is protein level and outcome is the complex trait or disease. Colors indicate the type of
1234 complex trait or disease. Cancer types were harmonized under a single “Cancer” group. Ancestry
1235 is denoted by filled circle (European), filled diamond (African), and filled square (East Asian). Each
1236 data point is plotted based on the chromosome and transcription start-site of the protein-coding
1237 gene. For simplicity, *Z* scores and *P* values are averaged across cohorts in the European ancestry
1238 plot and the African ancestry plot and shown as a single data point. In European ancestry, only
1239 associations that were consistent across all cohorts are shown.
1240



1241
 1242
 1243 **Extended Data Fig. 6. Uniquely instrumentable protein-phenotype pairs in African and East**
 1244 **Asian ancestries.**

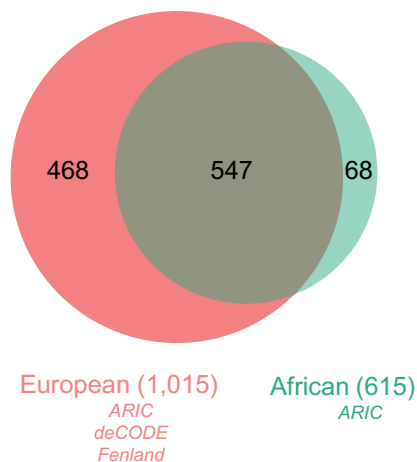
1245 Red arrows indicate a positive causal estimate of the protein on the outcome while blue arrows
 1246 indicate a negative causal estimate of the protein on the outcome.

1247 (a) Protein-phenotype pairs from 4 proteins uniquely instrumentable in African ancestry.
 1248 Significant estimates between proteins (orange circles) and traits (green rectangles).

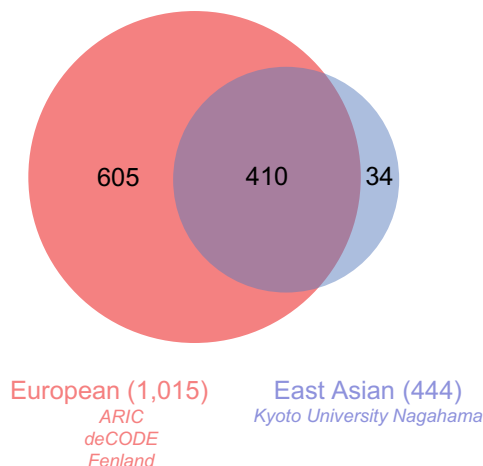
1249 (b) Protein-phenotype pairs from 8 proteins uniquely instrumentable in East Asian ancestry.
 1250 Significant estimates between proteins (orange circles) and traits (green rectangles).

1251

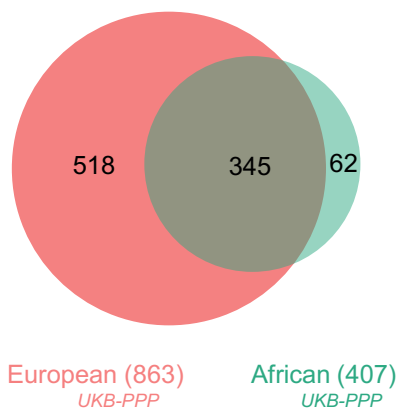
a SomaScan v4 European vs. African ancestry



b SomaScan v4 European vs. East Asian ancestry



c Olink Explore 3072 European vs. African ancestry



1252 **Extended Data Fig. 7. Cross-ancestry comparison stratified by proteomics platform of**
 1253 **instrumentable proteins overlapping at least one drug database (druggable genome,**
 1254 **DrugBank, or Open Targets Platform).**

1255 (a) Comparison of SomaScan v4 platform instrumentable proteins overlapping at least one drug
 1256 database between three European cohorts (ARIC, deCODE, and Fenland) and one African cohort
 1257 (ARIC).
 1258

1259 (b) Comparison of SomaScan v4 platform instrumentable proteins overlapping at least one drug
 1260 database between three European cohorts (ARIC, deCODE, and Fenland) and one East Asian
 1261 cohort (Kyoto University Nagahama).

1262 (c) Comparison of Olink Explore 3072 platform instrumentable proteins overlapping at least one
 1263 drug database between one European cohort (UKB-PPP) and one African cohort (UKB-PPP).
 1264

1265 **References**

- 1266 1. Sun, B. B. *et al.* Genomic atlas of the human plasma proteome. *Nature* **558**, 73–
1267 79 (2018).
- 1268 2. Emilsson, V. *et al.* Co-regulatory networks of human serum proteins link genetics
1269 to disease. *Science* **361**, 769–773 (2018).
- 1270 3. Suhre, K. *et al.* Connecting genetic risk to disease end points through the human
1271 blood plasma proteome. *Nat Commun* **8**, 14357 (2017).
- 1272 4. Williams, S. A. *et al.* Plasma protein patterns as comprehensive indicators of
1273 health. *Nat Med* **25**, 1851–1857 (2019).
- 1274 5. Su, C.-Y. *et al.* Circulating proteins to predict COVID-19 severity. *Sci Rep* **13**,
1275 6236 (2023).
- 1276 6. Carrasco-Zanini, J. *et al.* Proteomic signatures improve risk prediction for
1277 common and rare diseases. *Nat Med* **30**, 2489–2498 (2024).
- 1278 7. Hopkins, A. L. & Groom, C. R. The druggable genome. *Nat Rev Drug Discov* **1**,
1279 727–730 (2002).
- 1280 8. Overington, J. P., Al-Lazikani, B. & Hopkins, A. L. How many drug targets are
1281 there? *Nat Rev Drug Discov* **5**, 993–996 (2006).
- 1282 9. Bakheet, T. M. & Doig, A. J. Properties and identification of human protein drug
1283 targets. *Bioinformatics* **25**, 451–457 (2009).
- 1284 10. Santos, R. *et al.* A comprehensive map of molecular drug targets. *Nat Rev Drug*
1285 *Discov* **16**, 19–34 (2017).
- 1286 11. Pietzner, M. *et al.* Mapping the proteo-genomic convergence of human diseases.
1287 *Science* **374**, eabj1541 (2021).
- 1288 12. Ferkingstad, E. *et al.* Large-scale integration of the plasma proteome with
1289 genetics and disease. *Nat Genet* **53**, 1712–1721 (2021).
- 1290 13. Zhang, J. *et al.* Plasma proteome analyses in individuals of European and
1291 African ancestry identify cis-pQTLs and models for proteome-wide association
1292 studies. *Nat Genet* **54**, 593–602 (2022).
- 1293 14. Sun, B. B. *et al.* Plasma proteomic associations with genetics and health in the
1294 UK Biobank. *Nature* **622**, 329–338 (2023).
- 1295 15. Skrivankova, V. W. *et al.* Strengthening the reporting of observational studies in
1296 epidemiology using mendelian randomisation (STROBE-MR): explanation and
1297 elaboration. *BMJ* **375**, n2233 (2021).
- 1298 16. Skrivankova, V. W. *et al.* Strengthening the Reporting of Observational Studies in
1299 Epidemiology Using Mendelian Randomization: The STROBE-MR Statement. *JAMA*
1300 **326**, 1614–1621 (2021).
- 1301 17. Chong, M. *et al.* Novel Drug Targets for Ischemic Stroke Identified Through
1302 Mendelian Randomization Analysis of the Blood Proteome. *Circulation* **140**, 819–830
1303 (2019).
- 1304 18. Zheng, J. *et al.* Phenome-wide Mendelian randomization mapping the influence
1305 of the plasma proteome on complex diseases. *Nat Genet* **52**, 1122–1131 (2020).
- 1306 19. Zhao, H. *et al.* Proteome-wide Mendelian randomization in global biobank meta-
1307 analysis reveals multi-ancestry drug targets for common diseases. *Cell Genomics* **2**,
1308 100195 (2022).
- 1309 20. Zhou, S. *et al.* A Neanderthal OAS1 isoform protects individuals of European
1310 ancestry against COVID-19 susceptibility and severity. *Nat Med* **27**, 659–667 (2021).

- 1311 21. Yoshiji, S. *et al.* Proteome-wide Mendelian randomization implicates
1312 nephronectin as an actionable mediator of the effect of obesity on COVID-19 severity.
1313 *Nat Metab* **5**, 248–264 (2023).
- 1314 22. Yoshiji, S. *et al.* COL6A3-derived endotrophin mediates the effect of obesity on
1315 coronary artery disease: an integrative proteogenomics analysis.
1316 2023.04.19.23288706 Preprint at <https://doi.org/10.1101/2023.04.19.23288706>
1317 (2023).
- 1318 23. Lu, T., Forgetta, V., Greenwood, C. M. T., Zhou, S. & Richards, J. B. Circulating
1319 Proteins Influencing Psychiatric Disease: A Mendelian Randomization Study.
1320 *Biological Psychiatry* **93**, 82–91 (2023).
- 1321 24. Katz, D. H. *et al.* Whole Genome Sequence Analysis of the Plasma Proteome in
1322 Black Adults Provides Novel Insights Into Cardiovascular Disease. *Circulation* **145**,
1323 357–370 (2022).
- 1324 25. Wang, B. *et al.* Comparative studies of genetic and phenotypic associations for
1325 2,168 plasma proteins measured by two affinity-based platforms in 4,000 Chinese
1326 adults. 2023.12.01.23299236 Preprint at
1327 <https://doi.org/10.1101/2023.12.01.23299236> (2023).
- 1328 26. Said, S. *et al.* Ancestry diversity in the genetic determinants of the human plasma
1329 proteome and associated new drug targets. 2023.11.13.23298365 Preprint at
1330 <https://doi.org/10.1101/2023.11.13.23298365> (2023).
- 1331 27. Sakaue, S. *et al.* A cross-population atlas of genetic associations for 220 human
1332 phenotypes. *Nat Genet* **53**, 1415–1424 (2021).
- 1333 28. Feng, Y.-C. A. *et al.* Taiwan Biobank: A rich biomedical research database of the
1334 Taiwanese population. *Cell Genomics* **2**, 100197 (2022).
- 1335 29. Carlson, C. S. *et al.* Generalization and Dilution of Association Results from
1336 European GWAS in Populations of Non-European Ancestry: The PAGE Study. *PLOS*
1337 *Biology* **11**, e1001661 (2013).
- 1338 30. Martin, A. R. *et al.* Human Demographic History Impacts Genetic Risk Prediction
1339 across Diverse Populations. *The American Journal of Human Genetics* **100**, 635–649
1340 (2017).
- 1341 31. Cohen, J. *et al.* Low LDL cholesterol in individuals of African descent resulting
1342 from frequent nonsense mutations in PCSK9. *Nat Genet* **37**, 161–165 (2005).
- 1343 32. Robinson, J. G. *et al.* Efficacy and Safety of Alirocumab in Reducing Lipids and
1344 Cardiovascular Events. *New England Journal of Medicine* **372**, 1489–1499 (2015).
- 1345 33. Sabatine, M. S. *et al.* Evolocumab and Clinical Outcomes in Patients with
1346 Cardiovascular Disease. *New England Journal of Medicine* **376**, 1713–1722 (2017).
- 1347 34. Fatumo, S. *et al.* A roadmap to increase diversity in genomic studies. *Nat Med*
1348 **28**, 243–250 (2022).
- 1349 35. Ghoussaini, M. *et al.* Open Targets Genetics: systematic identification of trait-
1350 associated genes using large-scale genetics and functional genomics. *Nucleic Acids*
1351 *Research* **49**, D1311–D1320 (2021).
- 1352 36. Robinson, J. W. *et al.* An efficient and robust tool for colocalisation: Pair-wise
1353 Conditional and Colocalisation (PWCoCo). 2022.08.08.503158 Preprint at
1354 <https://doi.org/10.1101/2022.08.08.503158> (2022).
- 1355 37. Zhang, W. *et al.* SharePro: an accurate and efficient genetic colocalization
1356 method accounting for multiple causal signals. *Bioinformatics* **40**, btae295 (2024).

- 1357 38. Finan, C. *et al.* The druggable genome and support for target identification and
1358 validation in drug development. *Science Translational Medicine* **9**, eaag1166 (2017).
- 1359 39. Wishart, D. S. *et al.* DrugBank: a comprehensive resource for in silico drug
1360 discovery and exploration. *Nucleic Acids Research* **34**, D668–D672 (2006).
- 1361 40. Koscielny, G. *et al.* Open Targets: a platform for therapeutic target identification
1362 and validation. *Nucleic Acids Research* **45**, D985–D994 (2017).
- 1363 41. Schmidt, A. F. *et al.* Genetic drug target validation using Mendelian
1364 randomisation. *Nat Commun* **11**, 3255 (2020).
- 1365 42. Gkatzionis, A., Burgess, S. & Newcombe, P. J. Statistical methods for cis-
1366 Mendelian randomization with two-sample summary-level data. *Genetic Epidemiology*
1367 **47**, 3–25 (2023).
- 1368 43. Lawlor, D. A., Harbord, R. M., Sterne, J. A. C., Timpson, N. & Davey Smith, G.
1369 Mendelian randomization: Using genes as instruments for making causal inferences
1370 in epidemiology. *Statistics in Medicine* **27**, 1133–1163 (2008).
- 1371 44. Karczewski, K. J. *et al.* The mutational constraint spectrum quantified from
1372 variation in 141,456 humans. *Nature* **581**, 434–443 (2020).
- 1373 45. Benjamini, Y. & Hochberg, Y. Controlling the False Discovery Rate: A Practical
1374 and Powerful Approach to Multiple Testing. *Journal of the Royal Statistical Society.*
1375 *Series B (Methodological)* **57**, 289–300 (1995).
- 1376 46. Zuber, V. *et al.* Combining evidence from Mendelian randomization and
1377 colocalization: Review and comparison of approaches. *The American Journal of*
1378 *Human Genetics* **109**, 767–782 (2022).
- 1379 47. van der Graaf, A. *et al.* Mendelian randomization while jointly modeling cis
1380 genetics identifies causal relationships between gene expression and lipids. *Nat*
1381 *Commun* **11**, 4930 (2020).
- 1382 48. Goruppi, S. *et al.* The ULK3 Kinase Is Critical for Convergent Control of Cancer-
1383 Associated Fibroblast Activation by CSL and GLI. *Cell Reports* **20**, 2468–2479
1384 (2017).
- 1385 49. Hodonsky, C. J. *et al.* Multi-ancestry genetic analysis of gene regulation in
1386 coronary arteries prioritizes disease risk loci. *Cell Genomics* **4**, 100465 (2024).
- 1387 50. Verstockt, B. *et al.* IL-12 and IL-23 pathway inhibition in inflammatory bowel
1388 disease. *Nat Rev Gastroenterol Hepatol* **20**, 433–446 (2023).
- 1389 51. O’Meara, E. *et al.* Independent Prognostic Value of Serum Soluble ST2
1390 Measurements in Patients With Heart Failure and a Reduced Ejection Fraction in the
1391 PARADIGM-HF Trial (Prospective Comparison of ARNI With ACEI to Determine
1392 Impact on Global Mortality and Morbidity in Heart Failure). *Circulation: Heart Failure*
1393 **11**, e004446 (2018).
- 1394 52. Jiang, Y. *et al.* An IL1RL1 genetic variant lowers soluble ST2 levels and the risk
1395 effects of APOE- ϵ 4 in female patients with Alzheimer’s disease. *Nat Aging* **2**, 616–
1396 634 (2022).
- 1397 53. England, E. *et al.* Tozorakimab (MEDI3506): an anti-IL-33 antibody that inhibits
1398 IL-33 signalling via ST2 and RAGE/EGFR to reduce inflammation and epithelial
1399 dysfunction. *Sci Rep* **13**, 9825 (2023).
- 1400 54. Cohen, S. B. The use of anakinra, an interleukin-1 receptor antagonist, in the
1401 treatment of rheumatoid arthritis. *Rheumatic Disease Clinics of North America* **30**,
1402 365–380 (2004).

- 1403 55. Aviram, M. *et al.* Paraoxonase inhibits high-density lipoprotein oxidation and
1404 preserves its functions. A possible peroxidative role for paraoxonase. *J Clin Invest*
1405 **101**, 1581–1590 (1998).
- 1406 56. Reddy, S. T. *et al.* Human Paraoxonase-3 Is an HDL-Associated Enzyme With
1407 Biological Activity Similar to Paraoxonase-1 Protein but Is Not Regulated by Oxidized
1408 Lipids. *Arteriosclerosis, Thrombosis, and Vascular Biology* **21**, 542–547 (2001).
- 1409 57. Verma, A. *et al.* Diversity and scale: Genetic architecture of 2068 traits in the VA
1410 Million Veteran Program. *Science* **385**, eadj1182 (2024).
- 1411 58. Banfi, C. *et al.* Prenylcysteine oxidase 1, an emerging player in atherosclerosis.
1412 *Commun Biol* **4**, 1–17 (2021).
- 1413 59. Rocnik, E. F., Liu, P., Sato, K., Walsh, K. & Vaziri, C. The Novel SPARC Family
1414 Member SMOC-2 Potentiates Angiogenic Growth Factor Activity*. *Journal of*
1415 *Biological Chemistry* **281**, 22855–22864 (2006).
- 1416 60. Bourgault, J. *et al.* Proteome-Wide Mendelian Randomization Identifies Causal
1417 Links Between Blood Proteins and Acute Pancreatitis. *Gastroenterology* **164**, 953-
1418 965.e3 (2023).
- 1419 61. Lafferty, M. J., Bradford, K. C., Erie, D. A. & Neher, S. B. Angiotensin-like
1420 Protein 4 Inhibition of Lipoprotein Lipase: EVIDENCE FOR REVERSIBLE COMPLEX
1421 FORMATION* *This work was supported by a grant from the Pew Foundation (to S.
1422 B. N.). *Journal of Biological Chemistry* **288**, 28524–28534 (2013).
- 1423 62. Wang, H. & Eckel, R. H. Lipoprotein lipase: from gene to obesity. *American*
1424 *Journal of Physiology-Endocrinology and Metabolism* **297**, E271–E288 (2009).
- 1425 63. Rosenson Robert S. *et al.* Zodasiran, an RNAi Therapeutic Targeting ANGPTL3,
1426 for Mixed Hyperlipidemia. *New England Journal of Medicine* **0**,.
- 1427 64. Suhre, K., McCarthy, M. I. & Schwenk, J. M. Genetics meets proteomics:
1428 perspectives for large population-based studies. *Nat Rev Genet* **22**, 19–37 (2021).
- 1429 65. Liu, Z. *et al.* Genetic architecture of the inflammatory bowel diseases across East
1430 Asian and European ancestries. *Nat Genet* **55**, 796–806 (2023).
- 1431 66. Kong, L. *et al.* The landscape of immune dysregulation in Crohn’s disease
1432 revealed through single-cell transcriptomic profiling in the ileum and colon. *Immunity*
1433 **56**, 444-458.e5 (2023).
- 1434 67. Massimino, L. *et al.* The Inflammatory Bowel Disease Transcriptome and
1435 Metatranscriptome Meta-Analysis (IBD TaMMA) framework. *Nat Comput Sci* **1**, 511–
1436 515 (2021).
- 1437 68. Hamilton, M. J., Frei, S. M. & Stevens, R. L. The Multifaceted Mast Cell in
1438 Inflammatory Bowel Disease. *Inflammatory Bowel Diseases* **20**, 2364–2378 (2014).
- 1439 69. Boeckxstaens, G. Mast cells and inflammatory bowel disease. *Current Opinion in*
1440 *Pharmacology* **25**, 45–49 (2015).
- 1441 70. Bycroft, C. *et al.* The UK Biobank resource with deep phenotyping and genomic
1442 data. *Nature* **562**, 203–209 (2018).
- 1443 71. Koenig, Z. *et al.* A harmonized public resource of deeply sequenced diverse
1444 human genomes. 2023.01.23.525248 Preprint at
1445 <https://doi.org/10.1101/2023.01.23.525248> (2024).
- 1446 72. Purcell, S. *et al.* PLINK: A Tool Set for Whole-Genome Association and
1447 Population-Based Linkage Analyses. *The American Journal of Human Genetics* **81**,
1448 559–575 (2007).

- 1449 73. Durinck, S. *et al.* BioMart and Bioconductor: a powerful link between biological
1450 databases and microarray data analysis. *Bioinformatics* **21**, 3439–3440 (2005).
- 1451 74. Butler-Laporte, G. *et al.* HLA allele-calling using multi-ancestry whole-exome
1452 sequencing from the UK Biobank identifies 129 novel associations in 11 autoimmune
1453 diseases. *Commun Biol* **6**, 1–17 (2023).
- 1454 75. Holmes, M. V., Richardson, T. G., FERENCE, B. A., Davies, N. M. & Davey Smith,
1455 G. Integrating genomics with biomarkers and therapeutic targets to invigorate
1456 cardiovascular drug development. *Nat Rev Cardiol* **18**, 435–453 (2021).
- 1457 76. McLaren, W. *et al.* The Ensembl Variant Effect Predictor. *Genome Biology* **17**,
1458 122 (2016).
- 1459 77. Hemani, G. *et al.* The MR-Base platform supports systematic causal inference
1460 across the human phenome. *eLife* **7**, e34408 (2018).
- 1461 78. Pierce, B. L., Ahsan, H. & VanderWeele, T. J. Power and instrument strength
1462 requirements for Mendelian randomization studies using multiple genetic variants.
1463 *International Journal of Epidemiology* **40**, 740–752 (2011).
- 1464 79. Hemani, G., Tilling, K. & Smith, G. D. Orienting the causal relationship between
1465 imprecisely measured traits using GWAS summary data. *PLOS Genetics* **13**,
1466 e1007081 (2017).
- 1467 80. Zhang, W. *et al.* SharePro: an accurate and efficient genetic colocalization
1468 method accounting for multiple causal signals. 2023.07.24.550431 Preprint at
1469 <https://doi.org/10.1101/2023.07.24.550431> (2023).
- 1470 81. Giambartolomei, C. *et al.* Bayesian Test for Colocalisation between Pairs of
1471 Genetic Association Studies Using Summary Statistics. *PLOS Genetics* **10**,
1472 e1004383 (2014).
- 1473 82. Conway, J. R., Lex, A. & Gehlenborg, N. UpSetR: an R package for the
1474 visualization of intersecting sets and their properties. *Bioinformatics* **33**, 2938–2940
1475 (2017).
- 1476 83. Pruim, R. J. *et al.* LocusZoom: regional visualization of genome-wide association
1477 scan results. *Bioinformatics* **26**, 2336–2337 (2010).
- 1478